ACS OMEGA

Open Access

http://pubs.acs.org/journal/acsodf

Article

Environmentally Friendly UV-C Excimer Light Source with Advanced Oxidation Process for Rapid Mineralization of Azo Dye in Wastewater

Kiran Ahlawat, Ramavtar Jangra, and Ram Prakash*

Cite This: *ACS Omega* 2024, 9, 15615−15632

Read Online

ACCESS | Metrics & More | Article Recommendations | Supporting Information

ABSTRACT: Wastewater discharged from the textile industry contains approximately 15% unfixed dyes, predominantly 60−70% azo dyes. These unfixed dyes are a major environmental concern due to their persistence and potential toxicity. In this paper, an environmentally friendly mercury-free XeI* excilamp emitting 253 nm UV light is reported, and the same has been utilized for the degradation of azo dyes using the advanced oxidation process (AOP) with TiO_2/H_2O_2. A new process is developed in which one electrode of excilamp is coated with TiO_2 nanoparticles that improves the efficiency of the dye degradation. Additionally, the effects of varying TiO_2 loading concentrations, XeI*-excimer light intensity, starting dye concentration, suspension pH, and H_2O_2 addition are examined. The outcomes of this study confirm 13 times faster degradation in XeI*-excimer/H_2O_2 than in XeI*-excimer/TiO_2, attributed to an abundance of hydroxyl radicals generated by the modified XeI*-excimer/H_2O_2. Also, the degradation of RB5 in the modified XeI*-excimer/H_2O_2 is 2.3 times faster as compared to that of the bare electrode XeI*-excimer/H_2O_2. A more than 95% reduction in chemical oxygen demand has been achieved in 40 min in the case of XeI*-excimer/H_2O_2. In this study, a maximum energy yield of 5712 mg/kWh is reported. Furthermore, a high degree of degradation is found in the alkaline medium (pH 10). Because textile effluent is highly alkaline, this result is significant, and direct treatment of azo dyes is possible. The use of the developed source in industrial applications appears to be highly promising based on testing on a real wastewater matrix. The treated effluent has been utilized to study its reusability for agricultural purposes on the germination of radish seeds in soil, and ∼26% enhanced germination has been observed compared to dye wastewater.

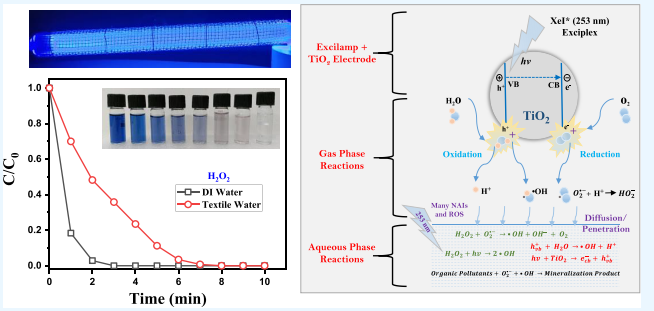

1. INTRODUCTION

To ensure compliance with environmental discharge regulations, wastewater quality assessment requires several components.[1] One significant issue that frequently causes wastewater to have a particular color is the presence of organic dyes. Textile effluents contain typical dye content ranging between 10 and 200 mg/L.[1] Many human and animal disorders have been traced to the toxic and highly carcinogenic nature of textile dyes.[2,3] A wide range of dyes exist, but because of their bright and long-lasting color, azo dyes (−N═N−) contribute 60 to 70% of the total dye consumed in the textile, paper, and leather industries.[4,5] These dyes are frequently utilized in industrial procedures, such as manufacturing artificial dyes and coloring materials in sectors like textiles, dry cleaning, and others.[6] Significant quantities of water are utilized in the textile industries for dying processes. Subsequently, color-rich wastewater is released at the various stages of the dying process,[1] necessitating the urgent development of closed-loop water supply systems to address concerns about resource usage. Also, because azo dyes are hydrolyzed,[7] they cannot be recovered for reuse and must therefore be degraded or eliminated before being released into the environment.

Various chemical, physical, and biological techniques are used to eliminate synthetic dyes from wastewater. These techniques include advanced oxidation process (AOP), adsorption, ultrafiltration, reverse osmosis, ion exchange, chlorination, ozone, aerobic, electro-Fenton, plasma treatment, and anaerobic.[8−14] Among them, AOPs such as ultraviolet light (UV) with H_2O_2/O_3 and photocatalysis are gaining popularity in removing complex organic pollutants from water and wastewater.[15−19] AOP accelerates the elimination of hazardous contaminants by creating highly reactive hydroxyl radicals (•OH).[20] The •OH is an extremely powerful, nonselective oxidant that causes partial or total mineralization of organic dye substances.[21] Among

Received: January 16, 2024
Revised: March 6, 2024
Accepted: March 8, 2024
Published: March 21, 2024

https://doi.org/10.1021/acsomega.4c00516
ACS Omega 2024, 9, 15615−15632

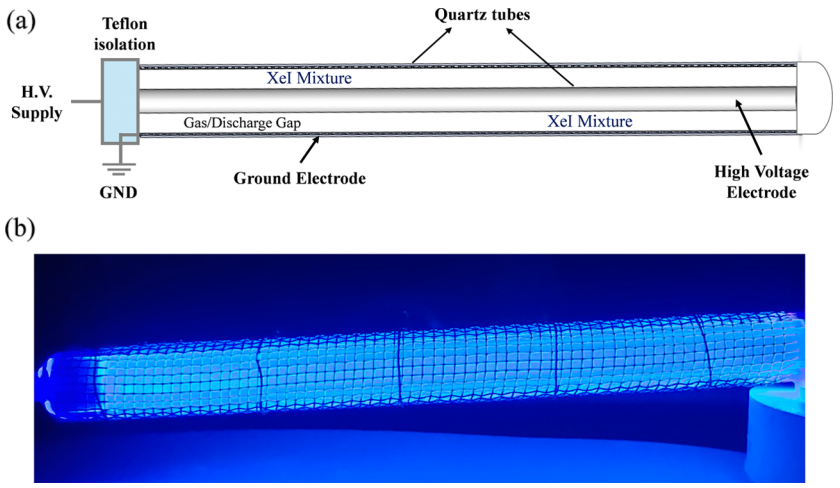

Figure 1. (a) Section view and (b) original view of the 253 nm mercury-free modified XeI*-excimer light source.

various AOPs, heterogeneous photocatalytic oxidation, particularly UV/TiO_2, is drawing a lot of attention.[22] TiO_2 is considered a more attractive choice for photocatalysts in environmental cleanup operations because of its low cost, high reactivity, high chemical stability, and nontoxic and insoluble nature.[23,24]

The most challenging problem in AOPs is the use of conventional UV light sources that often contain mercury, which is even more detrimental to the environment than the treated pollutants because of their routine replacement and frequent filament failure.[25,26] The best alternative to conventional mercury-based UV lamps is the dielectric barrier discharge (DBD) based mercury-free plasma UV excilamp.[27] Another difficulty related to AOPs is that, after the degradation process, the extraction and reuse of the catalysts from the treated matrix are quite challenging.[28] Recently, many research groups reported the immobilizing of photocatalysts directly onto the reactor walls to remove the organic dyes from the wastewater,[29,30] but the problem associated with this process is the decrease in photoactivity after certain cycles as well as the removal and replacement of photocatalysts from treated solution.[31,32] So, there is a need for process optimization, which eliminates the recovery and reuse of photocatalysts and simultaneously enhances the mineralization rate. According to Sun and Bolton,[33] H_2O_2 suspension shows a higher •OH radical generation rate and quantum yield than TiO_2 suspension; therefore, H_2O_2 can be considered as a radical promoter in photocatalytic applications.

Accordingly, excimer light sources based on the DBD combined with photocatalysts are being explored as a possible substitute to overcome these shortcomings. Excimer UV lamps are nontoxic (mercury-free), have instantaneous startup time, and are easily scalable and repairable. Such excilamps are an efficient source for water disinfection, dye degradation, and micropollutant removal.[27,34,35] Murcia et al.[36] performed the photodegradation of different dyes using XeBr, KrCl, and Cl_2 excilamps and found that KrCl excilamps show the best removal percentage followed by XeBr and Cl_2 excilamps. In another study by the same research group, two excilamps were compared in a UV/H_2O_2 process, and it concluded that excimer technology could be an excellent alternative to conventional methods.[37] In another study, Allabakshi et al. reported that azo dyes can be efficiently decomposed by using DBD in combination with a UV-C source,[38] and they concluded that this combination can overcome the quenching effect of •OH.

In this paper, the design and development of a mercury-free DBD-based modified XeI* excilamp are reported in which one of the electrodes is coated with TiO_2 nanoparticles to enhance the mineralization efficiency of the treated dye. This modified XeI*-excilamp generates 253 nm UV-C light and reactive oxygen species from the TiO_2 coated electrode simultaneously. The transportation mechanism of different active ions and reactive species from the gas phase to the aqueous phase has been discussed. The developed modified excilamp is the first of its kind and has been utilized to degrade RB5 azo dye effectively. The effects of different catalyst loadings, initial concentrations of dye, solution pH, and different concentrations of H_2O_2 are examined at different treatment times for the degradation of RB5 dye. Instead of loading photocatalysts in the wastewater suspension, we coated the TiO_2 on the electrode of the excilamp and utilized H_2O_2 as a radical promoter with varying concentrations of 0.013 to 0.039% v/v. To determine the toxicity of dye wastewater treated using various processes, radish seeds were germinated in soil using the treated dye wastewater and deionized water, and the results were analyzed. An understanding of how reactive species in the gas and aqueous phases interact with wastewater constituents and an effective strategy to valorize treated effluent are discussed.

The main components of uniqueness in this study are as follows:

1. A modified system (XeI* excilamp) that can simultaneously generate 253 nm UV light and the active ions and reactive species is developed.
2. By coating one of the electrodes of the excilamp with TiO_2 nanoparticles catalyst and diffusing the active ions and reactive species from the gas phase to the aqueous phase, the recovery step of photocatalysts is eliminated from the treated wastewater.
3. Accelerated degradation and mineralization of azo dye are reported when a modified excilamp is employed, and 0.04% v/v H_2O_2 is the only radical promoter used.
4. The role and mechanism of the active ions and reactive species generated from the TiO_2-coated mesh electrode in the degradation process are reported.
5. The modified XeI*-excimer/H_2O_2 treated wastewater has also been utilized for its phytotoxicity analysis on the germination of radish seeds.

https://doi.org/10.1021/acsomega.4c00516
ACS Omega 2024, 9, 15615−15632

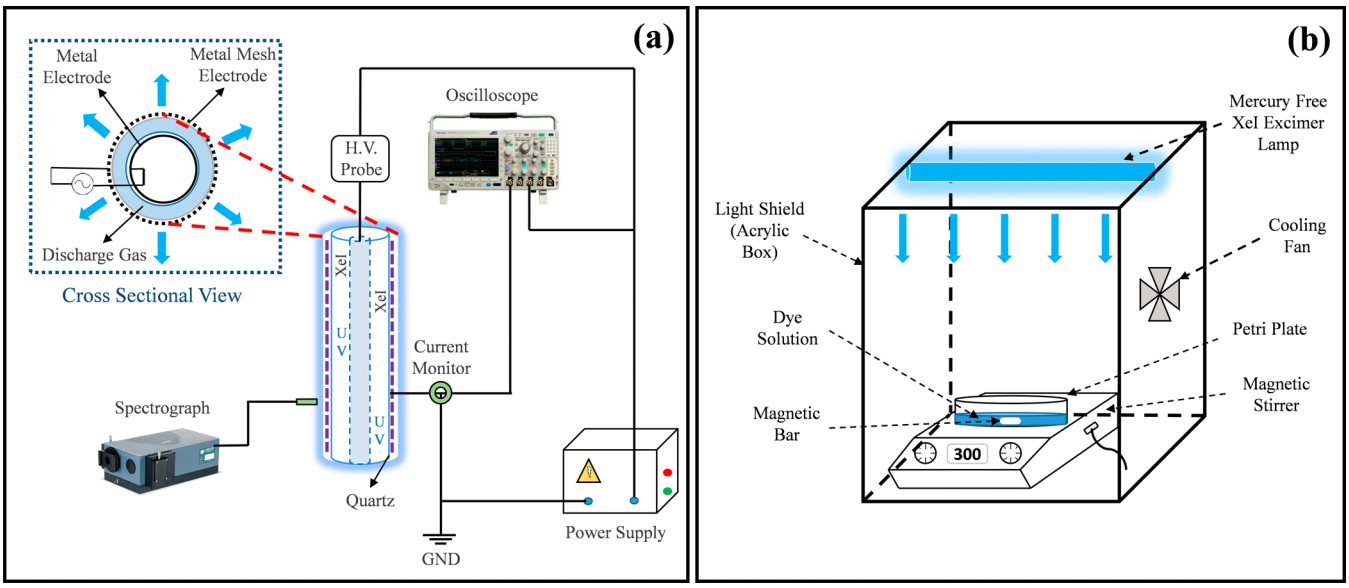

Figure 2. (a) Experimental setup of the developed mercury-free XeI* excimer light source equipped with electrical and optical measuring equipment. The dashed line box shows the cross-sectional view of the developed excimer source and (b) a schematic view of the experimental setup for mercury-free modified XeI* excilamp-based degradation of azo dye.

2. EXPERIMENTAL SETUP

2.1. Materials. Quartz tubes were purchased from QSIL GmbH (Germany), and reactive black 5 ($C_{26}H_{21}N_5Na_4O_{19}S_6$) and methylene blue ($C_{16}H_{18}N_3SCl$) dyes were purchased from Sigma-Aldrich and used without any further processing. Hydrogen peroxide (H_2O_2, 30% w/v), sodium hydroxide (NaOH, 97.0%), sulfuric acid (H_2SO_4, 97.0%), hydrochloric acid (HCL, 37%), benzoquinone ($C_6H_4O_2$, 98%), ammonium oxalate ($N_8H_4C_2O_4$, 99%), and isopropanol (IPA, C_3H_8O), and iodine crystal were purchased from Sigma-Aldrich. Research-grade xenon gas (99.99%) was procured from Phoenix Gases Pvt. Ltd., India, and argon gas (99.99%) was procured from The Scientific and General Agencies, India. Titanium dioxide (TiO_2) nanoparticles were synthesized in the laboratory. All of the stock solutions were prepared in deionized (DI) water and artificial wastewater. A mercury-free modified XeI*-excimer UV-C (253 nm) lamp was developed using standard laboratory practices.[39]

2.2. Excimer UV Source Design. The developed DBD-based XeI* UV-C excimer light source is shown in Figure 1. The inner and outer tube dimensions are 10 mm OD and 7 mm ID, and 16 mm OD, and 13 mm ID, respectively, and the lamp length is 160 mm. A wire mesh of stainless steel having a thickness of 0.1 mm coated with TiO_2 nanoparticles is used on the outer surface of the larger OD quartz tube, which acts as the ground electrode. An aluminum rod inserted inside the smaller quartz tube acts as a high-voltage electrode in the coaxial DBD configuration. This electrode is hermetically sealed for electrical isolation. The sectional and original view of the developed excimer source can be seen in Figure 1a,b, respectively. The development of a mercury-free modified XeI*-excimer light source consisted of multiple parts; first, the gas gap was evacuated up to 1×10^6 mbar of base pressure using a roughing vacuum pump and turbo molecular pump. After evacuation, the source was flushed with inert gases (argon and xenon) in a controlled manner before the desired pressure of the xenon and iodine mixture. The source was again evacuated up to the above-mentioned base pressure, and the gases were controlled by needle valves. Research-grade xenon gas (99.99%) was used, and a fraction of iodine was introduced for plasma formation in the lamp. The iodine concentration was optimized experimentally by varying its concentration from 5 to 0.0005% xenon for optimum UV-C radiations. The xenon gas pressure of 200 mbar was optimized in the experiment, along with a petite iodine concentration of 0.005% of xenon gas. Finally, the optimized lamp was pinched for further experimentation.

The developed mercury-free excilamp was operated by a bipolar pulsed power supply [1−10 kV, 10−40 kHz, 1 A, 2 μs pulse width] at different power settings. The power supply was grounded properly to avoid any electrostatic gathering. For the visualization of voltage and current waveforms, a high-voltage probe (Tektronix P6015A, 1000X) and a current monitor (Pearson 110, 0.1 V/A) were connected to a four-channel mixed domain oscilloscope (Tektronix MDO3014, 100 MHz, 2.5 GS/s). A calibrated thermocouple and IR camera were used to measure the temperature of the excimer source during experimentation.

When the excimer source is powered with high voltage, the excitation of the gases takes place, and the formation of XeI* excimer molecules occurs. Within a few nanoseconds of excitation, these excimer molecules decompose and release UV photons at 253 nm, with some weak transitions at other wavelengths. The length of the developed XeI* excilamp was 15 cm with an outer diameter of 1.6 cm, which corresponds to a surface area of 76 cm^2 for UV output radiation. An Andor PMT-based monochromator (SR-500i-B1) equipped with an optical fiber (200 μm, Ocean Optics) was used for analyzing the optical properties of the developed excimer source. A grating with 2400 grooves/mm was used to record the optical spectra of developed mercury-free XeI*-excilamp from 200 to 320 nm. For the measurement of the absolute intensity (in mW/cm^2) of the UV light from the excimer source, a Hamamatsu UV power meter (C9536) was used with a sensor head (H9535) precalibrated at the 254 nm wavelength. For the optical and electrical characterization of the developed excimer source, a complete experimental setup is shown in Figure 2a.

https://doi.org/10.1021/acsomega.4c00516
ACS Omega 2024, 9, 15615−15632

2.3. Preparation of TiO_2 Nanoparticle Powder and Its Coating onto the Outer Electrode. The photocatalytic activity of any catalyst strongly depends on its phase and crystalline size.[40,41] In this study, the TiO_2 nanoparticles were prepared by the sol−gel method, and the detailed method of preparation and advantage are discussed in our previous work[42,43] as well as in Section 1.1 of the Supporting Information (SI). The prepared TiO_2 nanoparticle solution was coated on the stainless-steel wire mesh electrode by a dip coating process, and the coated electrode was then annealed at 450 °C for 3 h to achieve strong coating. To confirm the nanoparticle formation, the prepared TiO_2 nanoparticle solution was annealed further at 450 °C for 3 h, and the obtained powder was analyzed using electron microscopy and UV−vis spectroscopy. The optical bandgap (E_g) energy of the synthesized nanoparticles was determined using the Tauc equation and Kubelka−Munk method,[44] which can be expressed as

$$(\alpha h\nu)^n = A(h\nu - E_g) \tag{1}$$

$$F(R) = \frac{(1-R)^2}{2R} \tag{2}$$

where $F(R)$ is the Kubelka−Munk function, equivalent to the absorption coefficient (α). By plotting the quantity of $[F(R)h\nu]^{1/2}$ against the photon energy ($h\nu$), the band gap of the nanoparticles was estimated. The band gap of 3.2 eV confirms the anatase phase of the TiO_2 nanoparticles. The field emission scanning electron micrograph (FE-SEM) and high-resolution tunneling electron microscopy (HRTEM) demonstrate the crystalline size of the nanoparticles. The stability of the coating on the mesh electrode was confirmed by performing a Scotch tape test.

The structural analysis of the synthesized material was done using an X-ray diffractometer (XRD) with Cu Kα radiation (λ = 1.54 Å), and data were collected for the two theta range of 20−80° at 0.02° step size. X-ray photoelectron spectroscopy (XPS: monochromatic Al Kα source, Thermo Fisher Scientific, USA) studies were performed to observe the surface properties and chemical states of the synthesized material.

2.4. Procedure and Analysis of Dye Degradation. All experiments were performed in the batch reactor, as shown in Figure 2b. A solution of different concentrations of the RB5 dye in DI water and artificial wastewater was chosen as a potential pollutant. An acrylic closed chamber of 1 × 1 × 1 cubic feet was used to house the developed mercury-free modified XeI*-excilamp and dye solution. The internal walls of the reaction chamber were covered with aluminum foil to reflect maximum UV irradiation onto the solution. The lamp was integrated into the upper portion of the chamber. A Petri plate with a diameter of 15 cm and a capacity of holding 500 mL of solution was placed on a magnetic stirrer, and a suspension of RB5 dye was transferred into it. UV-C irradiation was provided by using the developed mercury-free excimer source. The 5 mL samples from the suspension were withdrawn at regular intervals and immediately centrifuged at 3000 rpm for 15 min to remove catalyst particles entirely if loaded.

The effect of different XeI* excilamp intensities and impact of initial dye concentration (10, 30, 50, 70, and 90 mg/L), different catalyst loading (0.5, 0.75, 1, and 1.25 g/L), different pH (acidic, ambient, and alkaline), and different H_2O_2 concentrations (1, 3, and 5 mM) were analyzed to realize the degradation kinetics of the RB5 azo dye.

For the catalyst loading experiments, the required amount of TiO_2 was added, and the resulting catalyst suspension was magnetically stirred for 30 min in the dark to ensure complete equilibration of adsorption/desorption of RB5 on the TiO_2 surface. In most cases, experiments were performed at ambient solution pH, which were left unconstrained during the photocatalytic reaction. For experiments conducted under acidic or alkaline conditions, the initial pH was adjusted by adding the relevant quantity of H_2SO_4/HCL or NaOH, respectively. When the experiments were performed in the presence of H_2O_2, an appropriate amount of 35% w/v solution of H_2O_2 was added to attain the desirable concentration. All of the experiments were performed at ambient temperature, and all other parameters were kept the same throughout. Experiments were repeated more than three times, and the average values were plotted.

A UV−vis spectrophotometer (PerkinElmer, USA) was used to measure the RB5 dye concentration at its maximum absorbance (λ_{max} = 598 nm). High-resolution mass spectroscopy (HR-MS) and Fourier transform infrared spectroscopy (FTIR) were also used to analyze the degradation mechanism. A Vertex 70 V + PMA50 spectrophotometer (Bruker, USA) was used to record the FTIR spectra of untreated and treated day samples. The IR absorption spectra were recorded in the wavelength region of 4000−500 cm^{-1} with 32 scans at a resolution of 4.0 cm^{-1}. The RB5 degradation profile was confirmed by HR-MS analysis (Agilent 6500 Q-TOF LC/MS System). For this purpose, the samples were filtered and mixed with a final dilution of 1 mL of methanol/ACN (LC/MS grade) and introduced into an HR-MS equipped with a Dual AJS ion source operating in positive ionization mode in an ESI scan. All samples were analyzed using the following conditions: 50 °C dry gas temperature, 180 μL/h flow rate, capillary voltage of 5 kV, and nebulizer gas (N_2) pressure of 4.0 bar with a dry gas flow of 4.0 L/min. The mass range was m/z 200−1000 for all analyses, and 200 scans were acquired. Finally, the collected data were processed using suitable HR-MS software analysis.

The dye degradation efficiency, energy yield, and COD reduction were estimated using the following relationships:[45,46]

$$\text{Degradation efficiency}(\%) = \frac{C_0 - C_t}{C_0} \times 100 \tag{3}$$

$$\text{Energy yield, } Y\left(\frac{\text{mg}}{\text{kWh}}\right) = \frac{C_0 \times V \times D}{P \times t} \tag{4}$$

$$\text{COD reduction}(\%) = \frac{COD_0 - COD_t}{COD_0} \tag{5}$$

where C_0 is the initial concentration of the dye (mg/L), C_t is the dye concentration after treatment time t (mg/L), V is the volume of solution treated (L), D is the fraction of pollutant removed at a time t, P is the input power (kW), t is the treatment time (hour), COD_0 is the initial value of chemical oxygen demand (mg/L), and COD_t is the value of chemical oxygen demand after treatment time t (mg/L).

2.5. Assessment of the Reusability and Toxicity of the Treated Dye Wastewater. The toxicity effect of the untreated and treated dye effluents was assessed by employing their utility in the germination of radish seeds. The germination of the radish seeds was carried out using five different water samples, including DI water, untreated dye wastewater, treated dye wastewater with XeI* excimer/H_2O_2 (3 mM) for 3 and 40 min, and treated dye wastewater with XeI* excimer/TiO_2 (1 g/L).

https://doi.org/10.1021/acsomega.4c00516
ACS Omega 2024, 9, 15615−15632

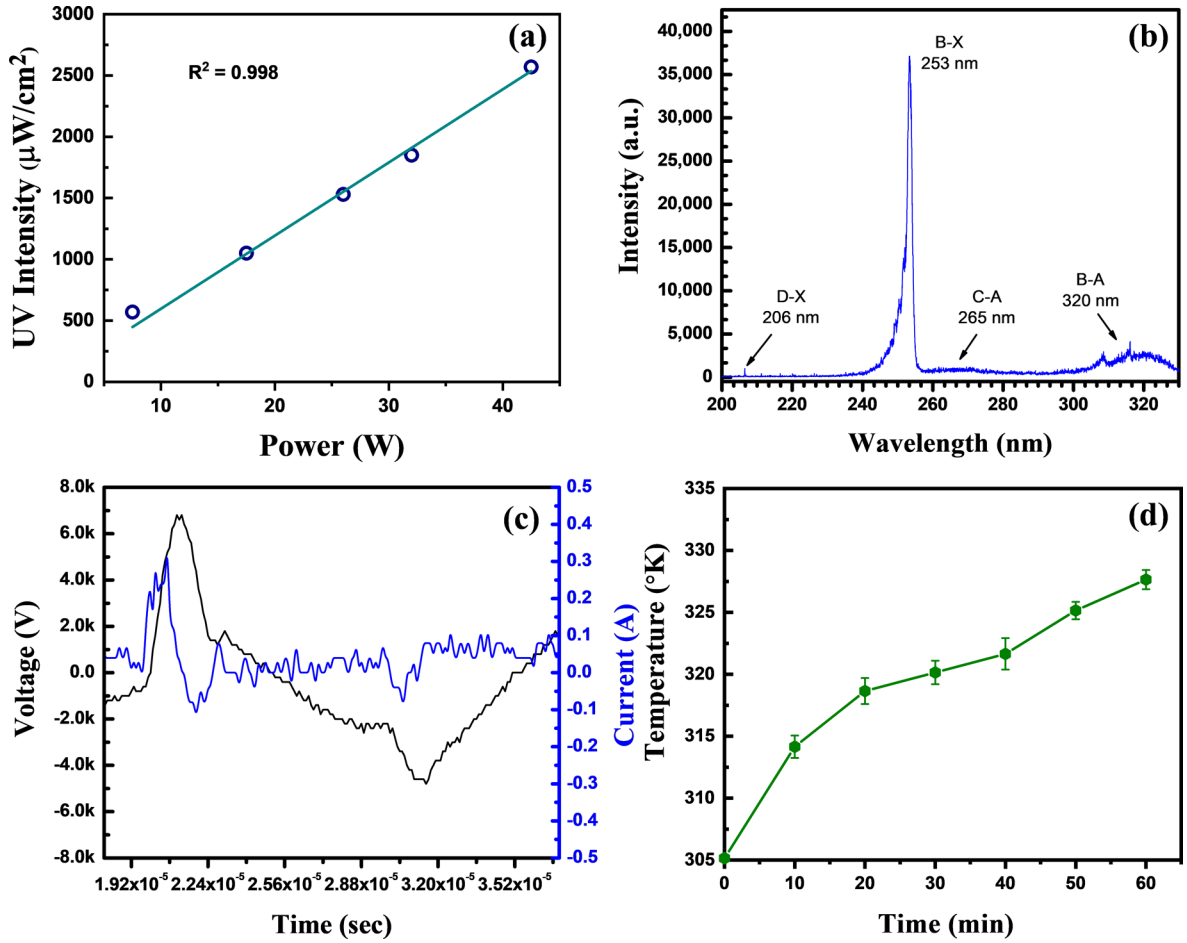

Figure 3. (a) Absolute XeI* excilamp intensity with respect to discharge power of the excimer source, (b) OES spectra of the excimer source dominating at wavelength 253 nm, (c) typical $V-I$ characteristics of the developed source, and (d) temperature variation of the treated solution as a function of XeI* excimer treatment time.

The pH of the solution used was neutral; therefore, we did not perform the neutralization of the treated effluents. The seeds were directly sown in the soil, and treated wastewater was used to water the soil to see the effect of different liquids on the growth of the stem and root of the radish seeds. This study was carried out for 3 days, and the impact of the different treated and untreated dye wastewater on the germination rate, stem length, and root length of the radish seed was studied.

3. RESULTS AND DISCUSSION

3.1. Excilamp Characterization. The photocatalytic activity and dye degradation rate strongly depend upon the intensity and wavelength of the UV light source used.[47] The absolute intensity of the developed UV-C (253 nm) lamp is shown in Figure 3a as a function of discharge power (W). It can be seen that the intensity increases linearly with increasing input power ($R^2 > 0.99$), and the time required to stabilize the UV intensity was about 30 s. A maximum of 2570 μW/cm^2 UV-C intensity is obtained at 42.5 W. All of the experiments of RB5 dye degradation are performed at an absolute UV intensity of 1050 μW/cm^2 (optimized based on gas pressure, applied voltage, and lamp heating) unless specifically mentioned. The optical emission spectra (OES) of the developed DBD-based excilamp are shown in Figure 3b. A prominent 253 nm spectral band corresponding to the B-X transition for XeI* along with some weak transition bands at 206 nm (D-X transition for I_2), 265 nm (C-A transition for XeI*), and 320 nm (B-A transition) can be seen in Figure 3b. Along with the 253 nm spectral band, these weak bands also participate in the process of degradation of dyes by enhancing the generation of •OH.

The typical voltage−current ($V-I$) characteristic is shown in Figure 3c at an applied voltage of 7 kV and frequency of 25 kHz. The input power of the excilamp is estimated by multiplying the recorded voltage and current values in the $V-I$ characteristics and then integrating them over time.[48] The input power is found to be 17.5 W for the developed mercury-free excilamp at the optimized parameters with 1050 μW/cm^2 UV output. From the absolute intensity measurement, we found that the XeI* excimer light source has an instant startup with full radiation output, in contrast to the mercury-based UV-C lamp, which has a startup time of about 2.5 min.[49] Figure 3d shows the temporal variation of temperature of the treated dye solution with respect to the treatment time. Even after 60 min of UV exposure to the dye solution, the solution temperature remains well below 330 K, indicating the nonthermal nature of the treated solution.

3.2. Characterization of TiO_2 Nanoparticles. The size and morphological characteristics of the nanoparticles are determined prior to the dye degradation process using FE-SEM and HRTEM analysis, and results are shown in Figures 4a−c. Figure 4a shows the FE-SEM image of a segment of TiO_2 coated stainless steel wire mesh electrode at a magnification of 67× (scale bar: 1 mm). The coating of TiO_2 is clearly visible on

https://doi.org/10.1021/acsomega.4c00516
ACS Omega 2024, 9, 15615−15632

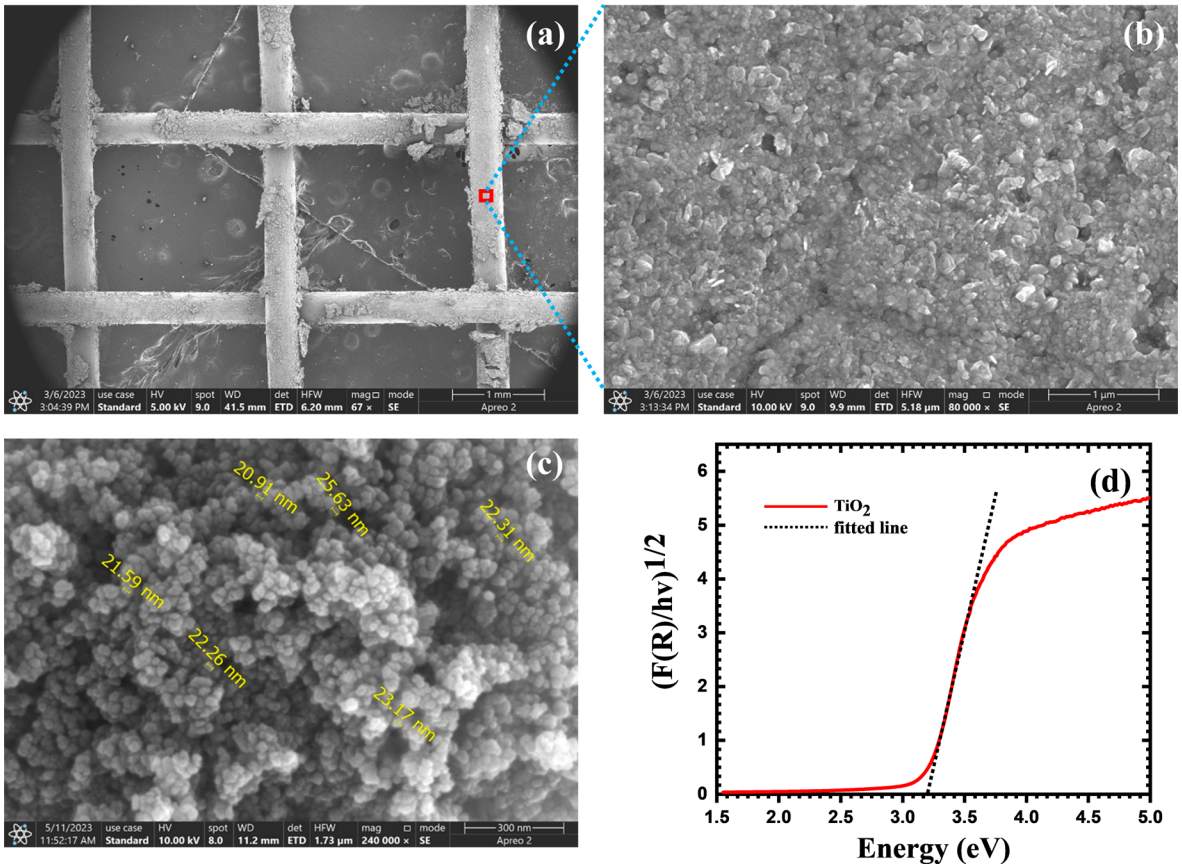

Figure 4. FE-SEM images of the TiO_2-coated outer mesh electrode at a magnification of (a) 67×, (b) 80,000×, and (c) FE-SEM image of synthesized TiO_2 nanoparticles (240,000×), and (d) the Kubelka−Munk plot of synthesized TiO_2 nanoparticles.

the mesh electrode. A high-magnification (80,000×, scale bar: 1 μm) image has also been captured by focusing on the single wire of the mesh electrode (see Figure 4b). To confirm the size of the nanoparticles, the FE-SEM of the TiO_2 nanopowder is also performed, and the obtained image can be seen in Figure 4c. The average size of the nanoparticles is ~23 ± 2 nm (as marked in Figure 4c) and is quite suitable for photocatalytic applications.[50] The Kubelka−Munk plot of synthesized TiO_2 nanoparticles is shown in Figure 4d, which confirms that the band gap of synthesized TiO_2 is 3.2 eV, corresponding to the anatase phage.[51] This phase of the TiO_2 nanoparticles is most suitable for photocatalytic applications in dye degradation.[52] The XRD pattern of the synthesized TiO_2 nanoparticles is shown in Figure S2.

Based on the HRTEM micrographs, spherical-like shapes with particle diameters of 20−30 nm could be seen for the synthesized TiO_2 nanoparticles (see Figure 5a). The variation in size between the nanoparticles obtained using the FE-SEM and HRTEM techniques might be attributed to both particle aggregation phenomena and the loss of nanoparticle stability during the freezing-drying process. The Image View software was used to analyze the particle size of the TiO_2, and measurement was taken over more than 60 particles. The historiographical representation of this measurement is shown in Figure 5b. To analyze the size, the Gaussian distribution was used. The surface properties and the changes in the chemical state can be evaluated using XPS. Figure 5c,d shows the XPS spectrum recorded for synthesized TiO_2. Two spectra are observed: one for the O 1s spectrum and the other for Ti 2p. The peak observed at 529.52 eV in Figure 5d is mainly observed for TiO_2. Another peak observed at 531.20 eV is possibly attributed to the adsorbed hydroxyl and oxygen ion; a broad peak suggests that they are weakly bound.[53] Figure 5c represents the spectrum of Ti 2p, in which two doublet peaks are observed, Ti 2p3/2 and Ti 2p1/2, at binding energies of 458.32 and 463.98 eV, respectively. This observed doublet is due to the spin−orbit coupling interaction.[54] Besides Ti and O, no other peak is observed, which suggests the phase purity of the synthesized TiO_2 nanoparticles.

3.3. Effect of Different Parameters on the Dye Degradation Efficiency. The effect of different parameters (initial dye concentration, pH, H_2O_2, and catalyst loading) on the degradation of the RB5 dye has been analyzed further. Figure 6a shows the chemical structure of the RB5 dye. The absorption spectra of the 50 mg/L RB5 dye solution as a function of different treatment times when exposed to excimer UV-C irradiation of intensity around 1 mW/cm^2 in the presence of 0.75 g/L TiO_2 loading at ambient pH are shown in Figure 6b. The RB5 dye has two broad and intense absorption bands at 312 nm in the UV region and 598 nm in the visible region; both have diminished upon exposure to the developed mercury-free XeI* excimer source. The intensity of the band at 598 nm is characteristic of the chromophore azo double bond of the RB5 dye. This intensity decreases rapidly when exposed to the UV-C excimer light, confirming approximately 90% degradation of the dye within 60 min of the treatment time and complete degradation in 90 min. A weak band in the UV-B region (312 nm) was also observed after 40 min, probably due to aromatic byproducts in the reaction medium.[55]

https://doi.org/10.1021/acsomega.4c00516
ACS Omega 2024, 9, 15615−15632

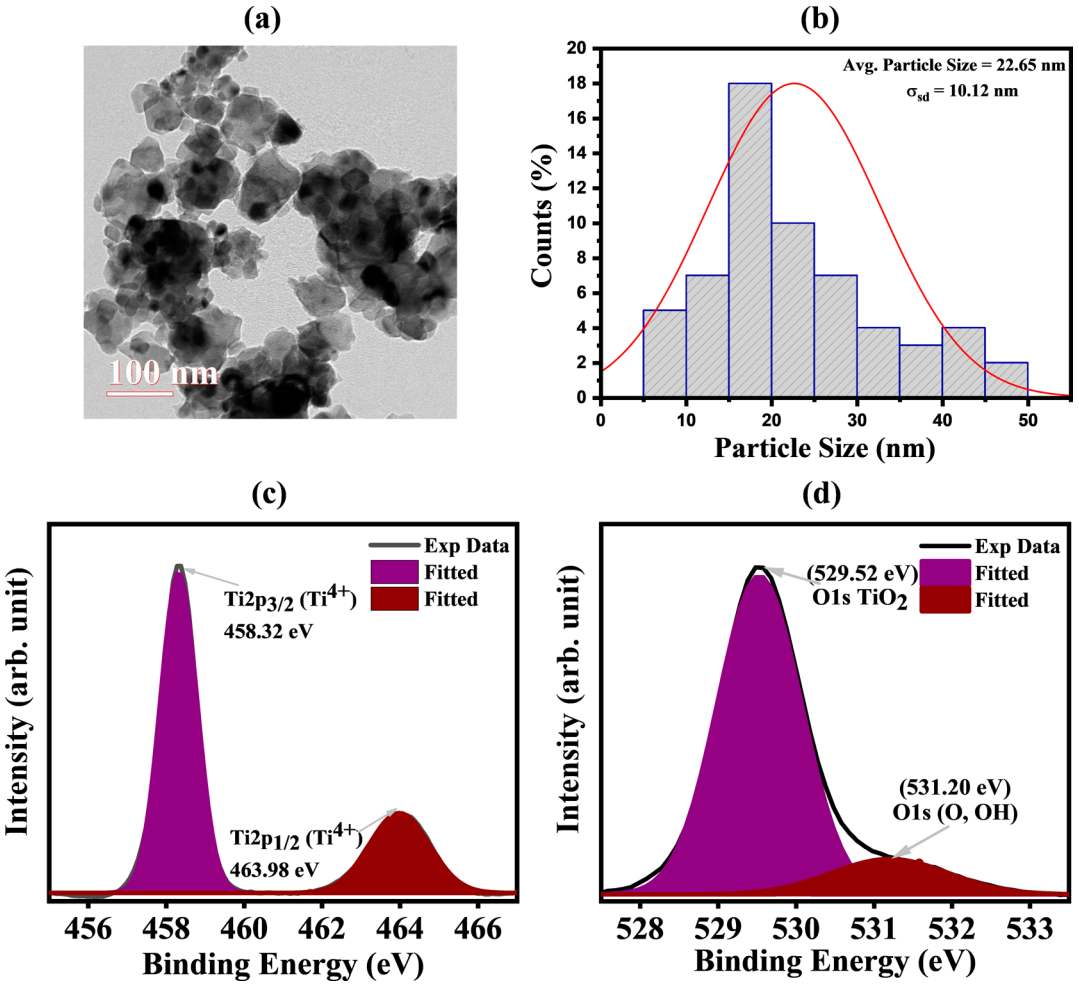

Figure 5. (a) Representative HRTEM micrographs of synthesized TiO_2 nanoparticles and (b) histogram representation with fitted Gausssian distribution for calculating TiO_2 nanoparticle average particle size. High-resolution XPS spectra of (c) Ti 2p and (d) O 1s in synthesized TiO_2 nanoparticles.

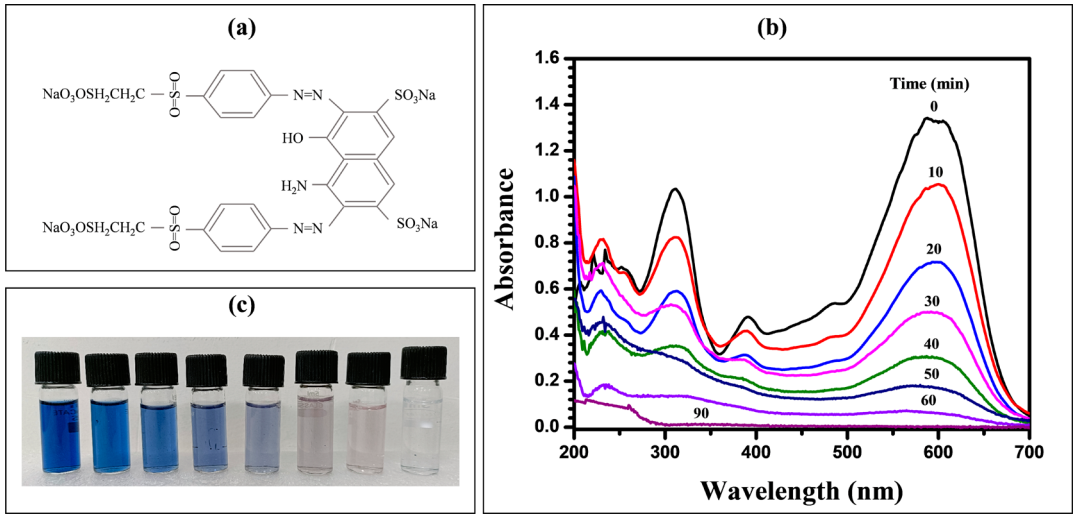

Figure 6. (a) Chemical structure of RB5 (MW 991.8), (b) UV−vis absorbance spectrum of the RB5 dye as a function of XeI* excimer light treatment time with 0.75g/L TiO_2 catalyst loading at ambient pH, and (c) pictorial representation of the degradation of the RB5 dye as a function of treatment time.

Figure 6c shows the pictorial representation of the decolorization of dyestuff at different exposure times by the developed excimer UV-C light source. A blank adsorption test was carried out in the dark by adding only 0.75g/L of TiO_2 in 50 mg/L of the dye suspension, and we found negligible degradation (<1%) in the initial concentration of the RB5.

https://doi.org/10.1021/acsomega.4c00516
ACS Omega 2024, 9, 15615−15632

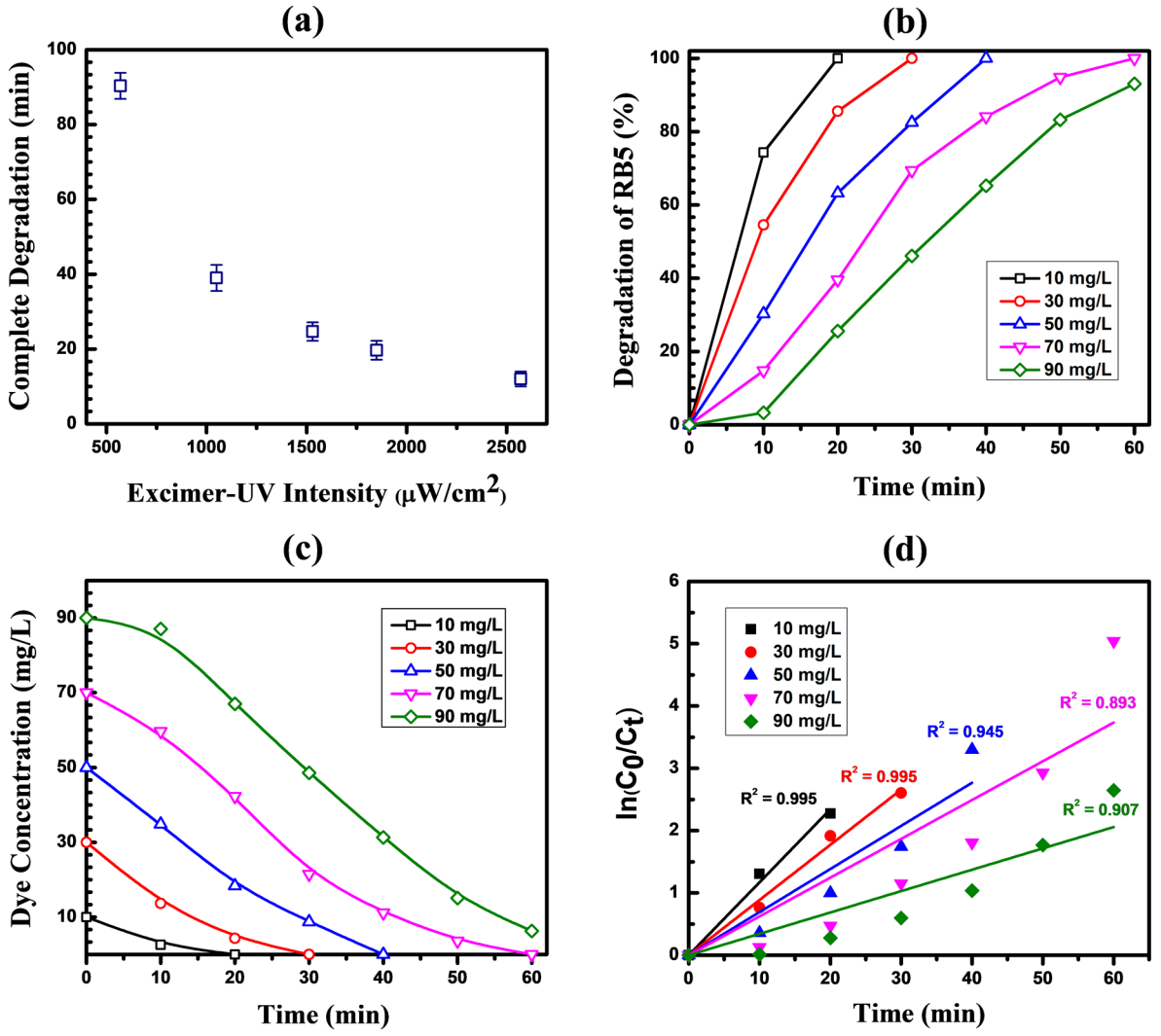

Figure 7. Effect of XeI* excimer light intensity on the (a) complete degradation of the RB5 dye (50 mg/L with 1g/L TiO_2 at ambient pH), (b) degradation as a function of exposure time with different initial concentrations of the RB5 dye with 1g/L TiO_2 at ambient pH, (c) residue dye concentration at different times, and (d) degradation under XeI*-excimer/TiO_2 processes based on a pseudo-first-order model.

The same test was performed in the visible light, and we found *a* < 2% reduction in the initial concentration of the dye after 60 min. It implies that the used dye is photostable in the visible range and is in agreement with the results published elsewhere.[55]

3.3.1. Effect of Excimer UV-C Intensity. The effect of excimer UV-C light intensity on RB5 dye degradation for the case of 50 mg/L dye concentration and 1 g/L TiO_2 loading at ambient pH is shown in Figure 7a. The effect of variation in light intensity has been studied in the range 550−2550 $\mu W/cm^2$. As can be seen in Figure 7a, the deterioration rate increases with increasing UV radiation intensity. This is because, with the increase in UV intensity, more UV-C photons fall on the catalyst surface, resulting in enhanced production of •OH, which leads to a high degradation rate[47,56] Liu et al.[57] experimented three different light intensities (1.24, 2.04, and 3.15 mW/cm^2) and found that the decolorization rate of the dye increases with increasing light intensity.

When the intensity was around 550 $\mu W/cm^2$, the dye completely degraded in about 90 min, and when the intensity was around 2550 $\mu W/cm^2$, the complete degradation of the dye took only 12 min. As mentioned above, for the developed mercury-free excilamp, the optimized UV-C intensity is 1050 $\mu W/cm^2$; therefore, all of the experiments of RB5 dye degradation are performed at an absolute UV intensity of 1050 $\mu W/cm^2$.

3.3.2. Effect of Initial Dye Concentration. The dependence of the photocatalytic process on the substrate concentration has also been investigated. The degradation is tested by varying the dye concentration from 10 to 90 mg/L and loading 1 g/L of TiO_2 catalyst at ambient pH. The acquired findings are shown in Figure 7b,c. For 50 mg/L, RB5 dye decomposed fully in just 40 min, whereas 90 mg/L degraded only ∼ 65% in the same period. It is evident that the higher the dye concentration is, the longer is the treatment time (see Figures 7b,c). For the increased dye concentration, less excimer UV-C photons could reach the photocatalyst surface, resulting in reduced •OH generation. The primary mechanism for •OH driven reactions is as follows:

$$TiO_2 + h\nu \rightarrow TiO_2(e^-) + TiO_2(h^+) \quad (6)$$

$$h^+ + H_2O \rightarrow \bullet OH + OH^+ \quad (7)$$

$$e^- + 0.5O_2 + H_2O \rightarrow \bullet OH + OH^- \quad (8)$$

$$h^+ + OH^- \rightarrow \bullet OH \quad (9)$$

https://doi.org/10.1021/acsomega.4c00516
ACS Omega 2024, 9, 15615−15632

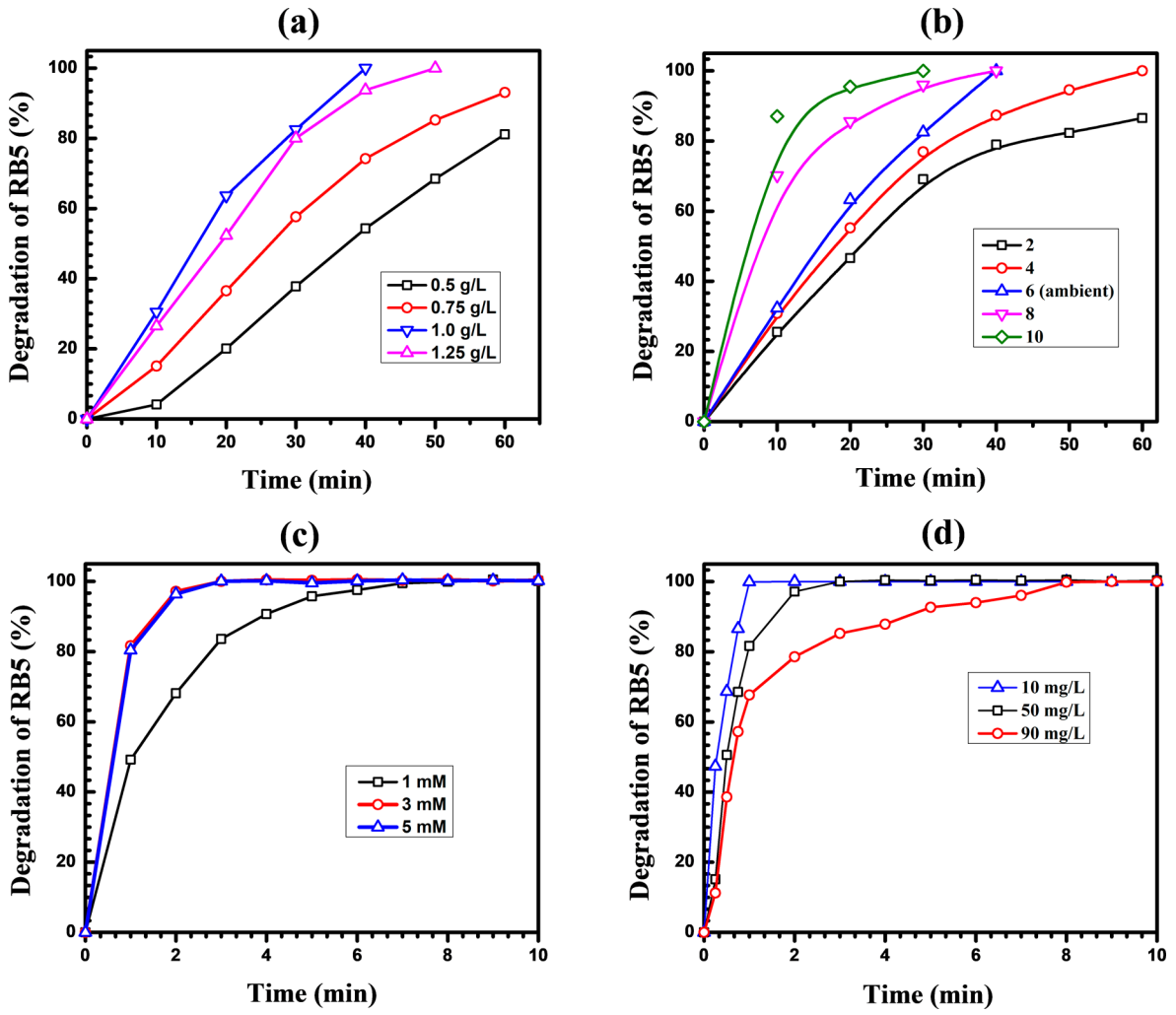

Figure 8. (a) Effect of different amounts of catalyst loading on RB5 dye degradation using the XeI* excimer light source at 50 mg/L initial dye concentration. (b) Effect of different pH values on RB5 dye degradation using the XeI* excimer light source at 50 mg/L initial dye concentration. (c) Effect of different concentrations of H_2O_2 on RB5 dye degradation using the XeI* excimer light source at 50 mg/L initial dye concentration. (d) Time course dye degradation with 3 mM H_2O_2 addition on different dye concentrations.

$$\text{RB5} + \text{OH}^{\bullet} \rightarrow \text{RB5}^{\bullet -} + \text{H}_2\text{O} \xrightarrow{\bullet\text{OH}} \text{degradation product} \quad (10)$$

In addition, there are indications that decolorization/degradation of suspension occurs by direct transfer of electrons and holes from the TiO_2 surface to the dye molecules[58,59] as follows:

$$\text{RB5} + \text{e}^{-} \rightarrow \text{RB5}^{\bullet -} \rightarrow \text{degradation product} \quad (11)$$

$$\text{RB5} + \text{h}^{+} \rightarrow \text{RB5}^{\bullet -} \rightarrow \text{degradation product} \quad (12)$$

So, as the dye concentration rises, photocatalyst activation decreases, resulting in fewer electrons available for direct reduction and fewer holes available for direct oxidation of the dye bond, further inhibiting degradation. The photocatalytic degradation of RB5 follows the pseudo-first-order kinetic model (see results in Figure 7d) and is expressed as shown in eq 13:[60]

$$\ln\left(\frac{C_0}{C_t}\right) = kt \quad (13)$$

where k is the first-order rate coefficient, C_0 is the initial concentration of the RB5 dye, and C_t is the RB5 dye concentration at time t. The value of C_t is obtained from Figure 7c. The obtained k values for 10, 30, 50, 70, and 90 mg/L are 0.1173, 0.0886, 0.0692, 0.0623, and 0.0343, respectively. The rate coefficient demonstrated linearity and validated the behavior of first-order kinetics. At low RB5 concentrations, the penetration of UV light into the aqueous solution is very high because of the lower concentration of dye molecules. However, when the dye concentration increases (70/90 mg/L), the degradation behavior deviates from first-order kinetics because of the lower penetration of UV light in the aqueous phase. This is because at high concentrations, the dye degradation rate is relatively slow at first. However, after 10 to 20 min of treatment, the rate of degradation increases because of reduced dye molecules. The obtained k values from this study are higher than the other reported k values for less than 75 mg/L dye concentration.[58]

3.3.3. Effect of TiO_2 Loading. Another important parameter for dye degradation studies is the catalyst loading. To determine the optimal amount of the catalyst dose, experiments have been performed at ambient pH by varying the amount of the catalyst from 0.5 to 1.25 g/L in 50 mg/L initial dye concentration. The effect of different concentrations of TiO_2 is shown in Figure 8a and the degradation efficiency increases continuously, with an

https://doi.org/10.1021/acsomega.4c00516
ACS Omega 2024, 9, 15615−15632

increase in the catalyst loading. However, the dye degradation efficiency decreased when the catalyst dose exceeded 1 g/L. At higher TiO_2 loading, the UV-C photon absorption increases, which results in more •OH production and increment of absorbance of dye molecules.[55] The increase in the photocatalytic performance with increasing TiO_2 loading is evidence of a heterogeneous catalytic phase. This is because the amount of incident light absorbed by TiO_2 increases with an increasing TiO_2 dosage in the suspension.

Interestingly, when the TiO_2 dose exceeded 1 to 1.25 g/L, the dye degradation efficiency declined. Perhaps the increased XeI* excimer light reflectance caused by the TiO_2 nanoparticles is mostly responsible for the decline in the RB5 dye degradation efficiency, as reported elsewhere.[61] We could identify an optimized concentration of TiO_2 catalysts as 1 g/L for 50 mg/L dye degradation when our advanced photocatalytic mercury-free excimer UV-C lamp is used. In a previous report, the optimized concentration of TiO_2 loading was 2 g/dm^3 in a solar/TiO_2 process, and the complete degradation was achieved in 200 min when the dye concentration was 3.85×10^{-4} M.[61]

The reusability and stability experiments of prepared TiO_2 nanoparticles have also been performed, and it was found that the prepared catalyst maintained good stability and reusability after five cycles of dye degradation (as shown in Figure S3). More information on reusability and stability can be found in Section 1.3 of the Supporting Information.

3.3.4. Effect of pH. The most important parameter that influences photocatalytic degradation is the pH of the solution.[58] Five different pH values in acidic, ambient, and alkaline media were studied to see the effect on the decolorization of the dye molecule at a fixed TiO_2 dose of 1 g/L. Figure 8b shows the percentage degradation of RB5 under acidic, ambient, and alkaline conditions. It can be observed from Figure 8b that degradation is much faster in the case of an alkaline medium than in an acidic medium. In just 20 min of treatment, the degradation has accelerated by 2-fold as the pH of a dye suspension rises from 2 to 10. This shows that the alkaline conditions are more favorable in our case. In general, the pH of the textile effluents is alkaline ($\sim 10 \pm 1$);[62] hence, these results hold an excellent opportunity to degrade the textile effluents more effectively.

The point of zero charge (PZC) for TiO_2 is 6.8. The surface of the catalyst is positively charged when the pH is below PZC and negatively charged when the pH is above PZC.[63] The RB5 dye is fully in anionic form within the pH range studied, i.e., due to the presence of sulfonic groups. With an increase in pH, the negative charges on TiO_2 are expected to repel the dye, and a decrease in photodegradation with increasing pH was expected. However, it has been observed that the RB5 dye degradation efficiency increases with an increased pH. A similar result was reported earlier for the RB5 dye and acid blue 40 dye degradation.[58] This effect may be attributed to the more efficient generation of •OH by TiO_2 with an increasing concentration of hydroxide ions. At pH values of 10 and 6 (ambient), the complete degradation of RB5 took around 30 and 40 min, respectively, making no significant contribution due to the alkalinity medium of the suspension. Accordingly, the ambient pH is selected for all of the experiments until mentioned.

3.3.5. Effect of the Addition of H_2O_2. Figure 8c shows the percentage degradation of the 50 mg/L RB5 dye profiles when the concentration of H_2O_2 has been varied at ambient pH (without any TiO_2 loading). For 1 mM concentration of H_2O_2, the complete degradation occurs in 7 min. In contrast, the degradation rate becomes constant for further increases in the H_2O_2 concentration, i.e., 3 and 5 mM, and complete degradation occurs in just 3 min of treatment. When we increased the concentration of H_2O_2, the degradation time decreased because of the higher •OH generation in the suspension. However, after a certain limit, the degradation rate becomes constant because H_2O_2 itself scavenges •OH (eq 14). Therefore, a high concentration of H_2O_2 does not provide a high degradation rate.

$$H_2O_2 + \bullet OH \rightarrow H_2O + HO_2^{\bullet} \quad (14)$$

The effect of H_2O_2 addition in a suspension containing 50 and 90 mg/L RB5 dye has been studied in further experiments. For 3 mM of H_2O_2 and the 90 mg/L dye solution, complete degradation occurs in 6 min. In contrast, when the same concentration of H_2O_2 in the 50 and 10 mg/L dyes is used, complete degradation occurs in 3 and 1 min, respectively (see Figure 8d). These results are due to the powerful oxidizing nature of H_2O_2, reacting rapidly with excimer UV-C light to produce •OH[58] or reacting with electrons to produce •OH and OH^-[23] through the following possible reactions:

$$H_2O_2 + h\nu \rightarrow 2\bullet OH \quad (15)$$

$$H_2O_2 + e^- \rightarrow \bullet OH + OH^- \quad (16)$$

$$H_2O_2 + 2h_{vb}^+ \rightarrow O_2 + 2H^+ \quad (17)$$

A dark test was also performed to check the degradation with only H_2O_2, and negligible degradation occurred in the aqueous dye solution, showing that the RB5 dye is quite stable under bleaching conditions. Moreover, adding TiO_2 into this process reduces the degradation efficiency because H_2O_2 scavenges the photogenerated oxidizing species, i.e., •OH and valence band holes (see eqs 14 and 17),[46] which would otherwise be available for the oxidative destruction of the dye molecules. Accordingly, XeI*-excimer/H_2O_2 is a preferable method of treating wastewater because of its ability to produce •OH (on-site) and also because it is a sludge-free operation with faster kinetics.[64]

3.3.6. Comparison and Mechanism of Degradation. Figure 9 compares XeI*-excimer/H_2O_2 performance with XeI*-excimer/TiO_2 and XeI*-excimer alone with different varying initial dye concentrations for complete degradation of the RB5 dye. The time taken for complete degradation of RB5 dye (50 mg/L) by a XeI*-excimer light source with TiO_2 is 40 min. On the other hand, with the XeI*-excimer source alone, it took

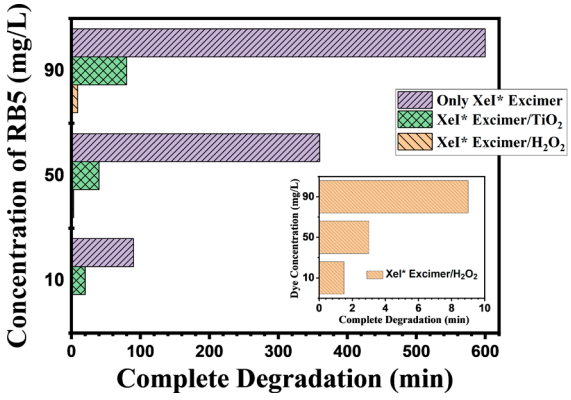

Figure 9. Time comparison of XeI*-excimer/H_2O_2 performance with XeI*-excimer/TiO_2 and XeI*-excimer alone at different varying initial dye concentrations for complete degradation of the RB5 dye.

https://doi.org/10.1021/acsomega.4c00516
ACS Omega 2024, 9, 15615−15632

Table 1. Comparison of Different Reactors for the Degradation of Various Organic Dyes

dye	dye conc. (mg/L)	sample volume (mL)	pH	light source and intensity	power (W)	process type & loading	time (min)	energy yield (mg/kWh)	degradation efficiency (%)	refs
RB5	200	100	6	medium-pressure UV lamp	250	UV/TiO_2 & 0.2 mg/L	240		96	65
Acid Orange 7	10	28 mL/min		240 white LEDs	60	LED/N-TiO_2, continuous flow			90	66
Rhodamine B	40	500	4	high-pressure mercury lamp (365 nm)	250	UV/TiO_2 flow process and 1 g/L	100		92	67
Methylene blue	20		6.8		19	multineedle to plane liquid DBD plasma	40	537	90–96	68
Brilliant Red 5B		100			95	photo SDBD	14	401	>99	5
RB5	50	100	6	XeI* excilamp and 1.050 mW/cm^2	17.5	UV/TiO_2 & 1 g/L	40	428.6	>99	this study
RB5	50	100	6	XeI* excilamp and 1.050 mW/cm^2	17.5	UV/H_2O_2 & 0.0137% v/v	3	5712	>99	this study

around 360 min. When H_2O_2 is added to the dye suspension and irradiated with XeI*-excimer light, it shows exceptional results, and complete degradation of RB5 dye takes only 3 min. This is perhaps due to the more significant production of •OH in XeI*-excimer/H_2O_2 because of the multiple electron transitions in the UV region (see Figure 3b) and the reaction mechanism (eqs 14−17) explained above. According to Sun and Bolton,[33] the •OH generation rate and the quantum yield for the TiO_2 suspension are much lower than the H_2O_2 suspension, which is also one of the reasons for the higher removal rate in the case of H_2O_2 than TiO_2.

A comparison of different UV-based reactors operated at different powers for the degradation of the RB5 dye is shown in Table 1. It reveals that the dye degradation time in advanced XeI*-excilamp/H_2O_2 is much less than that of the other UV-based reactors reported earlier in the literature.

In this study, the excitation of mesh electrode TiO_2 nanoparticles occurred when the XeI* excimer source transferred the energy (253 nm) to the surface of the catalyst. This reaction creates electron and hole pairs, which further react with atmospheric moisture (H_2O) and oxygen (O_2) to generate a pool of active ions and reactive species.[69] The concentrations of active air ions have been measured using an air ion counter (AIC 2, Alpha Lab, USA) and found to be ~15,000 ions/cm^3. The negative air ions have been utilized for the on-site production of •OH and other reactive species. As reported by Jiang et al.,[69] the lifetime of these negative air ions was found to be 100 s to several minutes. Luts and Salm[70] identified that superoxide ions (O_2^-) is the primary negatively charged ion and is more stable than other negative air ions. These photochemically generated negative air ions and reactive species can diffuse from the gas phase to the aqueous phase and further react with the different species present in the water, as shown in Figure 10. Various computational and experimental studies show the different scenarios of how these active ions and reactive species were transported from the gas phase to the aqueous phase.[71,72] In the nonexistence of electron and hole pairs in the suspension (because of absence of TiO_2), superoxide ions (from the modified XeI* excimer source) react with H_2O_2 and produce •OH, which are subsequently used for the mineralization of organic wastewater. A separate experiment has been performed without a TiO_2 mesh electrode to see the effect of only UV light on the photolysis of H_2O_2 for dye mineralization. Because of the low quantum yield of H_2O_2 at 253 nm,[35] the degradation rate decreases, and results are shown in Figure S4.

3.4. Radical Scavenging Effect. The modified XeI* excimer source-based degradation studies of the RB5 dye by

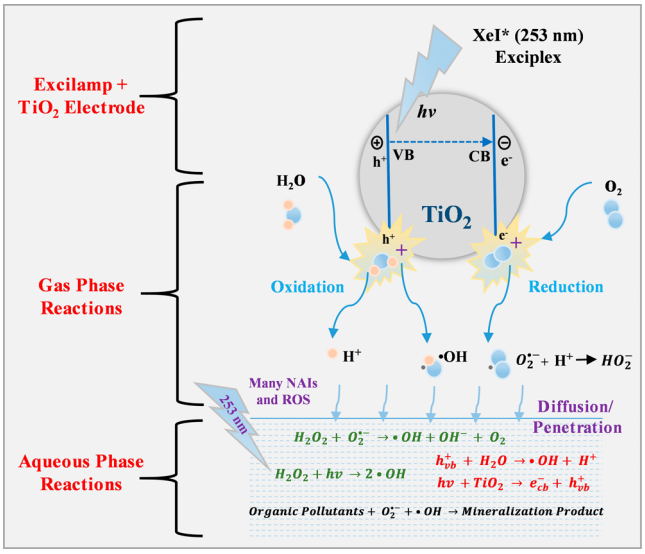

Figure 10. Proposed mechanism for the aqueous azo dye degradation using a modified XeI* excilamp.

adding H_2O_2 as a radical promotor are also confirmed by scavenging studies, as seen in Figure 11. These studies are used to examine the role of the reactive species in the modified XeI* excimer source-based degradation mechanism. Benzoquinone (BQ), ammonium oxalate (AO), and isopropanol (IPA) act as scavengers with active radicals $O_2^{\bullet-}$, h^+, and •OH, respectively.[73] The experiments are carried out using the modified XeI*

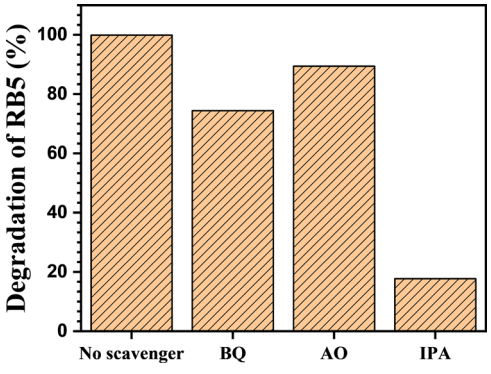

Figure 11. Quenching studies of reactive species during the modified XeI* excimer source based degradation of the RB5 dye over H_2O_2 as a radical promotor.

https://doi.org/10.1021/acsomega.4c00516
ACS Omega 2024, 9, 15615−15632

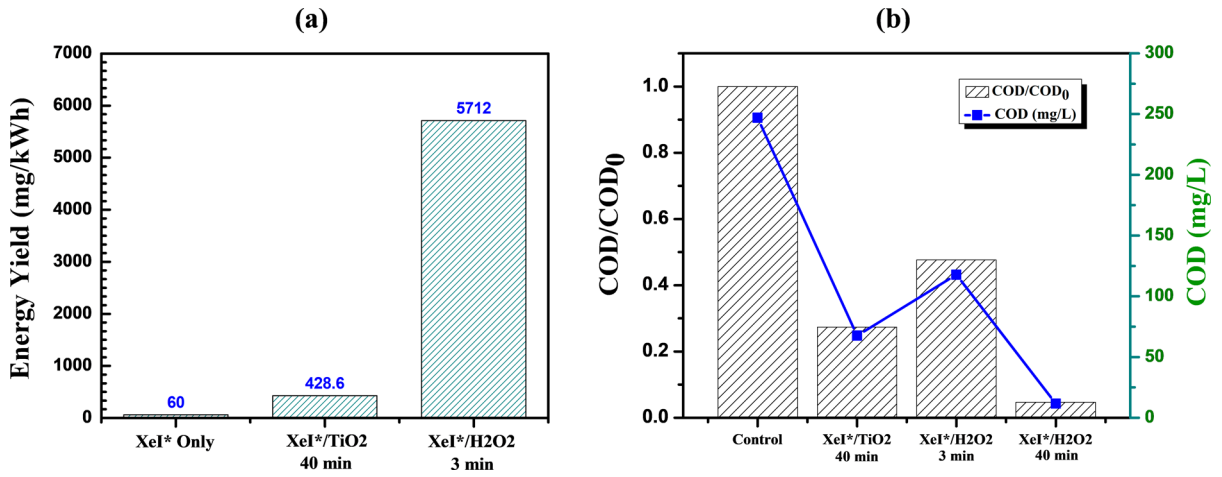

Figure 12. (a) Energy yield corresponding to different treatment methods for complete dye degradation (50 mg/L) and (b) COD removal as a function of treatment methods at ambient pH and initial RB5 dye concentration of 50 mg/L.

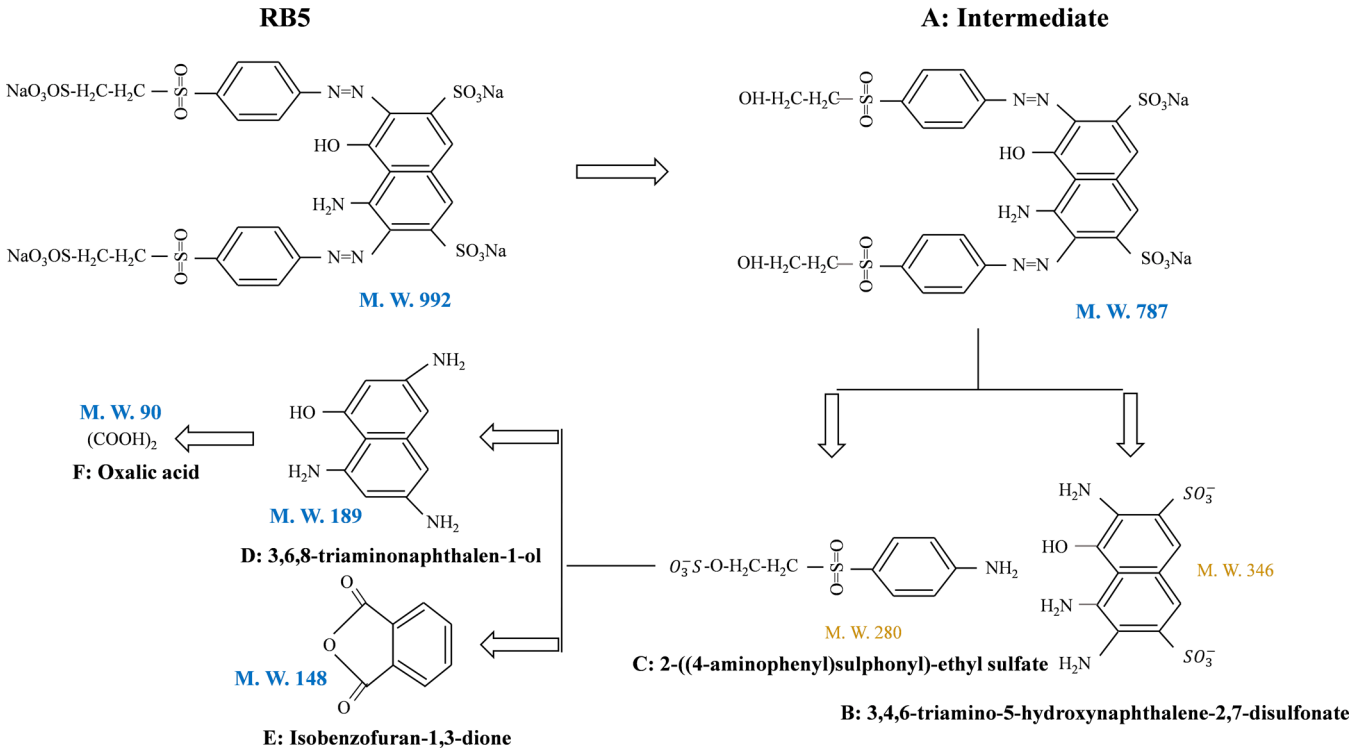

Figure 13. Possible degradation pathway of RB5 dye by the XeI* excimer light-assisted photocatalytic reaction.

excimer source without scavengers and with these three active radicals on the RB5 dye in the presence of H_2O_2 as a radical promotor. It is found that adding different scavengers considerably reduces the rate of RB5 degradation. After degradation, it exhibits 99.9, 74.4, 89.4, and 17.7% RB5 degradation for H_2O_2, BQ, AO, and IPA, respectively. Therefore, from this experiment, it is clearly observed that these three active radicals are involved in the degradation mechanism and the production of •OH.

3.5. Energy Yield and COD Analysis. Energy yield is a widely accepted parameter among the plasma-based water treatment methods to evaluate the energy efficiency of plasma-based reactors. In this study, the energy yield of a DBD plasma-based mercury-free excilamp is computed for different methods by using eq 4. For the complete degradation of dye, the maximum energy yield in the case of XeI*-excimer/TiO_2 is found to be 428.6 mg/kWh for 50 mg/L dye concentration and 1 g/L TiO_2. Meanwhile, the maximum energy yield in the case of XeI*-excimer/H_2O_2 is found to be 5712 mg/kWh for 50 mg/L dye concentration and 3 mM H_2O_2. Figure 12a shows the system's energy yield for different treatment methods used in this work. Allabakshi et al.[5] used a surface dielectric barrier discharge system with UV-C light for dye mineralization and reported a maximum energy yield of 522 mg/kWh. According to the literature, the present XeI*-excimer/H_2O_2 system showed reasonably good energy efficiency compared to many other reported plasma reactors.

The mineralization and toxicity of treated RB5 dye are estimated by the COD analysis of the untreated and treated dye solution. COD is a parameter that reflects the organic burden

https://doi.org/10.1021/acsomega.4c00516
ACS Omega 2024, 9, 15615−15632

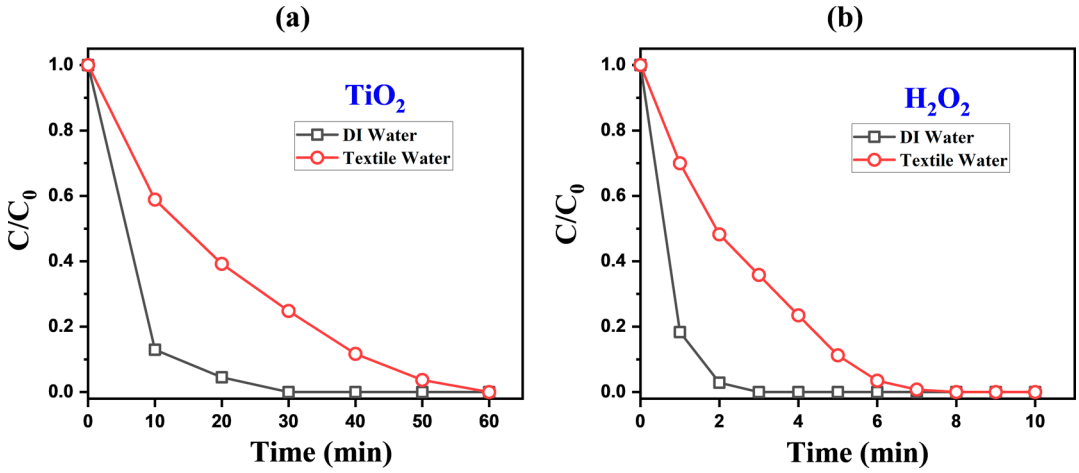

Figure 14. Comparison of degradation rates in DI water and textile water (a) with TiO_2 (initial RB5 concentration 50 mg/L, TiO_2 loading 1 g/L, and pH 10.4) and (b) with H_2O_2 (initial RB5 concentration 50 mg/L, H_2O_2 loading 3 mM, and pH 10.4).

and, by extension, the chemical concentration of effluents. Transformation of organic compounds into inorganic compounds reduces the COD and is directly related to the degradation of organic matter.[74] COD concentrations of 50 mg/L untreated dye solution and those treated with XeI*-excimer/TiO_2 for 40 min, XeI*-excimer/H_2O_2 for 3 min, and XeI*-excimer/H_2O_2 for 40 min at ambient pH are shown in Figure 12b. It is found that the initial COD concentration was 246.7 mg/L, and it declined to 67.68 mg/L after 40 min treatment with the XeI*-excimer/TiO_2 process. When COD is reduced by up to 72.6%, at that treatment time, the rate of RB5 dye removal is found to be ∼99.9%. In the case of 50 mg/L dye concentration and 3 mM H_2O_2, the COD is reduced by 52.3% in the treatment time of 3 min, and the rate of RB5 dye removal is found to be ∼99.9%. For more than 95% COD reduction, it will take 40 min in the case of 50 mg/L dye concentration and 3 mM H_2O_2. We find that for more mineralization, more treatment time is needed. Further, a significant decrease in COD values at the RB5 dye suspension treated with the excimer UV-C photocatalytic process indicated its potential for reactive azo dye degradation. The results hold a good promise for the rapid mineralization of the RB5 dye and can be an effective method for the treatment of RB5 dye.

3.6. Possible Degradation Pathway of RB5 Dye. Untreated and XeI*-excimer/H_2O_2 degraded RB5 dye samples are examined using HR-MS and FTIR techniques to determine a possible mechanism for RB5 dye degradation. The fragmentation data and m/z values obtained from mass spectroscopy analysis are used to identify the fragmented byproducts. Based on the intermediates of its degradation and earlier publications[65,75] a possible mechanism for the degradation of RB5 dye is proposed and shown in Figure 13. Degradation of RB5 dye follows multiple steps like dissociation of azo (−N═N−) bond, rearrangement of the functional group, ring opening, and finally its mineralization.

Initially, the breakage of the C−O bond in RB5 dye is caused by the •OH immediate interaction with organic contaminants that leads to the production of the intermediate as shown in A: Intermediate in Figure 13 (m/z 787). According to A: Intermediate, the breakdown of the azo bond leads to the creation of products B (m/z 346) and C (m/z 280), which are related with the direct degradation of RB5 dye through the UV-assisted photodegradation process. Further, fragmentation of product B results in the formation of product D (m/z 189) by the dissociation of the C−SO_3 bond. The fragmentation of product C results in the formation of product E (m/z 148), which mineralized into oxalic acid (m/z 90) through the ring opening mechanism of product E. The •OH attack on the benzene rings caused them to break, which then began the breakdown of the RB5 dye into less refractory intermediate molecules, eventually mineralizing into CO_2 and H_2O. It can be inferred that the degradation of dyes involves the cleavage of azo bonds, which results in the formation of aromatic amines followed by their complete disintegration.[65,76] The analytical data showed that the azo (N═N) bond in the RB5 dye has been degraded into several intermediate products.

3.7. Degradation Comparison with the Real Water Matrix. The widely used process for textile wastewater treatment is advanced photocatalytic oxidation. However, in this process, the extraction and reuse of the catalysts are challenging. We have eliminated the process of catalyst extraction and recovery by developing a modified XeI* excimer reactor for the faster degradation/mineralization of the azo dyes. The effects of the XeI* excimer reactor on the real water matrix (diluted seawater) have been investigated through a series of tests, and the outcomes are compared to the model RB5 degradation. The different parametric values of DI water and diluted seawater can be seen in Table S1. Figure 14 compares the degradation of the model RB5 solution to that of diluted seawater to demonstrate the effectiveness of the employed approach. Sea water was chosen as a textile effluent alternative due to the presence of high concentrations of salts because during the wet dying process, the textile industries use salts to enhance the penetration of the dye into the fabric and for dying efficiency.[77] The TiO_2 and H_2O_2 based XeI* excimer degradation rate of artificial textile water is lower than that of the model RB5 solution prepared with DI water, as can be seen in Figure 14a,b.

Textile effluent generally contains dissolved organic matter, as well as ions such as CO_3^{2-}, Ca^{2+}, K^+, Na^+, HCO_3^-, SO_4^{2-}, etc. All of these components react with •OH, thus reducing its concentration and making it less accessible for dye molecules. Also, •OH reacts with some inorganic ions, like HCO_3^- and SO_4^{2-}, and forms the corresponding radicals, such as $HCO_3^{\bullet}$ and $SO_4^{\bullet-}$, which are less efficient for oxidation as compared to •OH itself.[78] Still, the modified XeI* excimer reactor is very efficient

https://doi.org/10.1021/acsomega.4c00516
ACS Omega 2024, 9, 15615−15632

Table 2. Effect of Different Treatments of Dye Wastewater on Radish Seed Germination

	DI	dye wastewater	treated with TiO_2	treated with H_2O_2 for 3 min	treated with H_2O_2 for 40 min
stem length (cm)	7.086 ± 1.233	4.078 ± 1.015	7.054 ± 1.451	7.435 ± 1.098	9.88 ± 1.042
root length (cm)	1.277 ± 0.212	1.1 ± 0.183	1.222 ± 0.229	1.643 ± 0.209	2.16 ± 0.361
germination (%)	88	76	88	92	96

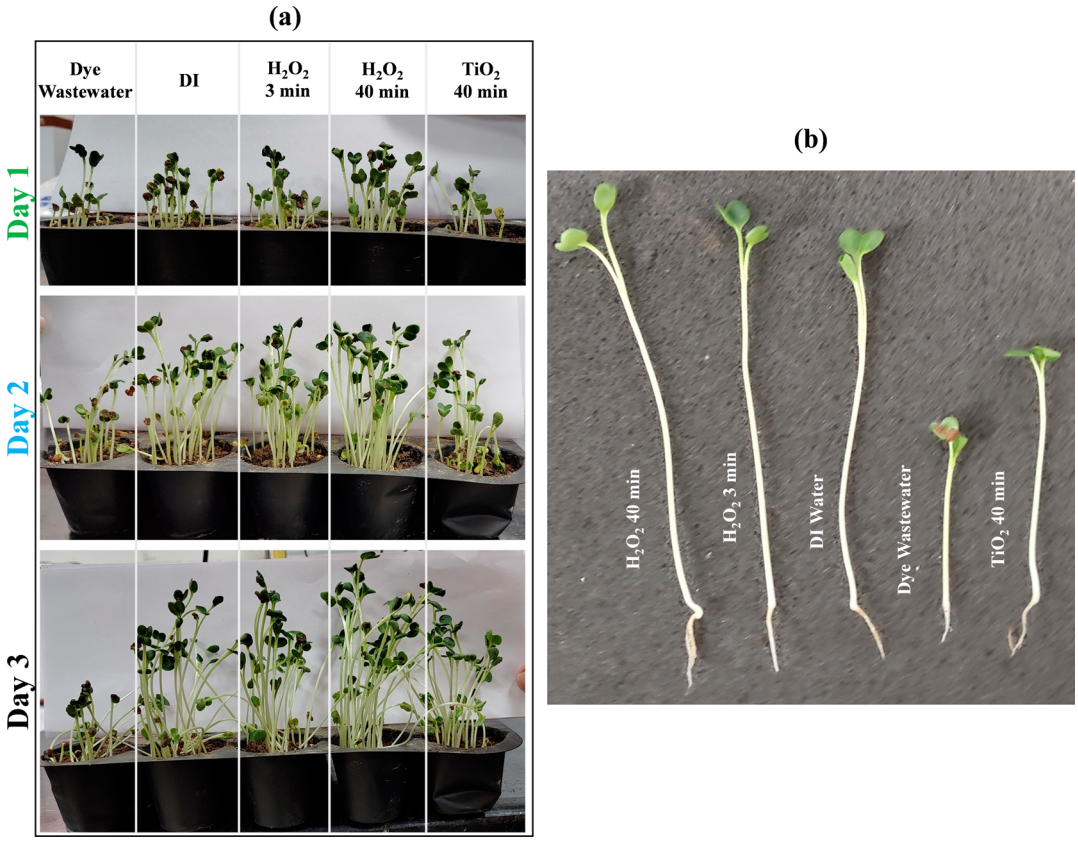

Figure 15. Photographic image of (a) of the growth of the radish seeds in soil for 3 days and (b) stem and root length after 3 days.

because the complete degradation has been achieved in just 7 min in the case of XeI*-excimer/H_2O_2. Because RB5 dye is an anionic dye, it has been further demonstrated that the excimer reactor that has been built is a superior alternative to traditional techniques; the degradation of a cationic dye (methylene blue) has also been performed. The results of this experiment have shown that the modified XeI* excimer source using H_2O_2 as a radical promoter successfully acts on the cationic dye as well, and after just 8 min of treatment, 99.99% of the 50 mg/L of methylene blue has been degraded. The UV−vis degradation profile of methylene blue and the corresponding degradation can be seen in Figure S5. A comparison of the degradation of RB5 with TiO_2/H_2O_2 in sunlight vs the modified XeI* source can also be seen in Figure S6.

3.6 Toxicity Analysis of Treated Effluents and Its Reusability for Agriculture Purposes. Radish seeds are first sown directly into the soil to evaluate the germination ability of the treated and untreated dye wastewater. The water resulting from the separate treatments using XeI*-excimer/TiO_2 and XeI*-excimer/H_2O_2 is then used for watering the seeds. The germination process is allowed to proceed for 3 days under controlled conditions. The seed germination ability of DI water, untreated dye wastewater, XeI*-excimer/H_2O_2 3 min treated dye wastewater, XeI*-excimer/H_2O_2 40 min treated dye wastewater, and XeI*-excimer/TiO_2 40 min treated dye wastewater is analyzed and compared by measuring the stem and root length. Table 2 summarizes the germination percentage, root length, and stem length after 3 days of incubation.

To illustrate it further, the images of the growth of the stem and roots of radish seeds during 3 continuous days of incubation are captured, which are shown in Figure 15. Figure 15a shows the growth of the radish seeds in soil for 3 days consecutively, and Figure 15b provides a visual representation of the impact of the various treatments on seed germination and growth (stem and root length) in a more natural and applicable context.

The study demonstrates that treating dye wastewater separately using XeI*-excimer/TiO_2 and XeI*-excimer/H_2O_2 under 253 nm light significantly enhances the degradation of the dye molecules. The water resulting from these separate treatments shows positive effects on radish seed germination and growth when compared to untreated dye wastewater. UV/H_2O_2 treated wastewater shows enhanced germination compared to DI water because some recent findings show that H_2O_2 can be used to increase the growth of the plant[79,80] On the other hand, when H_2O_2-dissolved wastewater is treated with a DBD-based modified XeI*-excimer source, various reactive oxygen species are produced, which also help in enhanced seed germination.[81] Germination of the seeds in the case of XeI*-excimer/H_2O_2 (40 min) is 98%, whereas in the case of XeI*-

https://doi.org/10.1021/acsomega.4c00516
ACS Omega 2024, 9, 15615−15632

excimer/TiO_2, it is found to be near 89% despite having the same treatment time. This can be due to the presence of more nondegraded dye in the XeI*-excimer/TiO_2 treated wastewater than the XeI*-excimer/H_2O_2 treated wastewater. The root length in the case of dye wastewater is quite less because of nutritional deficiency in the dye wastewater due to the presence of more organic contaminants. The pH in all of the experiments is found to be neutral; hence, no neutralization is required after treatment. In general, in direct atmospheric pressure cold plasma treatments, the pH of the treated effluents decreases, and it becomes acidic in nature.[5] However, in the direct photolysis process, no neutralization is required,[82] which is one of the advantages of this study. When we compare the growth in 3 and 40 min by XeI*-excimer/H_2O_2 treatment, the treatment for 40 min displayed the highest germination percentage and enhanced growth of stems and roots because of the increased demands of oxygen in the case of 3 min as compared to 40 min treatments (see Figure 12b). The above results suggest the potential use of a mercury-free plasma XeI*-excimer source for agricultural applications. Further research is needed to delve into the precise mechanisms underlying these effects and optimize the treatment process for wider environmental and agricultural applications.

CONCLUSIONS

In this work, an environmentally friendly XeI* excimer light source was developed and used for the degradation of RB5 dye with an advanced oxidation process using TiO_2 and H_2O_2. In the case of XeI*-excimer/TiO_2, the degradation of 50 mg/L of RB5 has been achieved in 40 min when the concentration of TiO_2 loading was 1 g/L at ambient pH. A faster degradation (within 3 min) of RB5 has been achieved by using the XeI*-excimer/H_2O_2 process in the case of 50 mg/L dye suspension at ambient pH. The mineralization of the dye has also been performed, and more than 95% removal in the COD concentration has been achieved within 40 min of the treatment with XeI*-excimer/H_2O_2. The order of degradation and mineralization is found to be XeI*-excimer/H_2O_2 > XeI*-excimer/TiO_2 > XeI*-excimer alone. The developed process is environmentally friendly (because of no mercury used) and eliminates the process of recovery of catalysts from the treated water after degradation. The faster degradation occurs in the alkaline medium (pH 10), which makes this process more favorable to use for the treatment of wastewater because the textile effluents have alkaline nature. The optimized method, i.e., XeI* excimer/H_2O_2, can be utilized for enhanced decolorization and mineralization of the unfixed dye in textile effluents. The results have been compared with existing dye degradation methods, and this environmentally friendly approach is found to be more effective in terms of time taken for degradation and energy yield. The treated water resulting from these separate treatments has been used on radish seed, and the seed germination and root growth have shown a positive impact as compared to untreated dye wastewater. The wastewater used for seed germination is the same as that obtained from the different processes in this study. Large-scale textile wastewater treatment is possible with the intended reactor; however, to ensure that the reactor is applicable in practice, extensive pilot-scale testing of the design is required. It is further required to conduct more research on the application of modified XeI* excimer sources for sustainable agriculture practices.

ASSOCIATED CONTENT

Data Availability Statement

The data sets generated and/or analyzed during the current study are available throughout the manuscript and supporting files.

Supporting Information

The Supporting Information is available free of charge at https://pubs.acs.org/doi/10.1021/acsomega.4c00516.

Preparation and advantage of TiO_2 nanoparticles, XRD, reusability and stability of TiO_2 nanoparticles, comparison of RB5 degradation under different electrode, different parameters value of treated water, methylene blue degradation profile, and comparison of RB5 degradation with sunlight (PDF)

AUTHOR INFORMATION

Corresponding Author

Ram Prakash − *Department of Physics, Indian Institute of Technology Jodhpur, Jodhpur, Rajasthan 342037, India;* orcid.org/0000-0003-3561-6801; Email: ramprakash@iitj.ac.in

Authors

Kiran Ahlawat − *Department of Physics, Indian Institute of Technology Jodhpur, Jodhpur, Rajasthan 342037, India*

Ramavtar Jangra − *Department of Physics, Indian Institute of Technology Jodhpur, Jodhpur, Rajasthan 342037, India*

Complete contact information is available at: https://pubs.acs.org/10.1021/acsomega.4c00516

Notes

The authors declare no competing financial interest.

ACKNOWLEDGMENTS

K.A. and R.J. would like to acknowledge the University Grants Commission (UGC) for providing senior research fellowship during the PhD program. All authors acknowledges the Core Research Grant (CRG), Science and Engineering Research Board (SERB), Department of Science and Technology (DST), Government of India, through project CRG/2020/005369 for the financial assistance of this work. The authors would like to thank Prof. Ambesh Dixit and Mr. Chandra Prakash for their support in the material synthesis and analysis during this study. The authors would also like to thank Prof. Meenu Chabra and Ms. Arti Sharma for their support in the COD analysis during this study.

REFERENCES

(1) Yaseen, D. A.; Scholz, M. Textile Dye Wastewater Characteristics and Constituents of Synthetic Effluents: A Critical Review. *Int. J. Environ. Sci. Technol.* **2019**, *16*, 1193 DOI: 10.1007/s13762-018-2130-z.

(2) Al-Tohamy, R.; Ali, S. S.; Li, F.; Okasha, K. M.; Mahmoud, Y. A. G.; Elsamahy, T.; Jiao, H.; Fu, Y.; Sun, J. A Critical Review on the Treatment of Dye-Containing Wastewater: Ecotoxicological and Health Concerns of Textile Dyes and Possible Remediation Approaches for Environmental Safety. *Ecotoxicol. Environ. Saf.* **2022**, *231*, No. 113160.

(3) Al-Mamun, M. R.; Kader, S.; Islam, M. S.; Khan, M. Z. H. Photocatalytic Activity Improvement and Application of UV-TiO2 Photocatalysis in Textile Wastewater Treatment: A Review. *J. Environ. Chem. Eng.* **2019**, *7* (5), No. 103248.

(4) Benkhaya, S.; M'rabet, S.; El Harfi, A. Classifications, Properties, Recent Synthesis and Applications of Azo Dyes. *Heliyon* **2020**, *6*, No. e03271, DOI: 10.1016/j.heliyon.2020.e03271.
(5) Allabakshi, S. M.; Srikar, P. S. N. S. R.; Gomosta, S.; Gangwar, R. K.; Maliyekkal, S. M. UV-C Photon Integrated Surface Dielectric Barrier Discharge Hybrid Reactor: A Novel and Energy-Efficient Route for Rapid Mineralisation of Aqueous Azo Dyes. *J. Hazard. Mater.* **2023**, *446*, No. 130639.
(6) Chandanshive, V.; Kadam, S.; Rane, N.; Jeon, B. H.; Jadhav, J.; Govindwar, S. In Situ Textile Wastewater Treatment in High Rate Transpiration System Furrows Planted with Aquatic Macrophytes and Floating Phytobeds. *Chemosphere* **2020**, *252*, No. 126513.
(7) Science, W.; El-dein, A. M.; Libra, J. A. Kinetics of Decolorization and Mineralization of the Azo Dye Reactive Black 5 by Hydrogen Peroxide and UV Light. *Water Sci. Technol.* **2001**, *44*, 295 DOI: 10.2166/wst.2001.0310.
(8) Kooshki, S.; Pareek, P.; Mentheour, R.; Janda, M.; Machala, Z. Efficient Treatment of Bio-Contaminated Wastewater Using Plasma Technology for Its Reuse in Sustainable Agriculture. *Environ. Technol. Innov.* **2023**, *32*, No. 103287.
(9) Lee, S. Y.; Kang, D.; Jeong, S.; Do, H. T.; Kim, J. H. Photocatalytic Degradation of Rhodamine B Dye by TiO2 and Gold Nanoparticles Supported on a Floating Porous Polydimethylsiloxane Sponge under Ultraviolet and Visible Light Irradiation. *ACS Omega* **2020**, *5* (8), 4233−4241.
(10) Lafi, R.; Gzara, L.; Lajimi, R. H.; Hafiane, A. Treatment of Textile Wastewater by a Hybrid Ultrafiltration/Electrodialysis Process. *Chem. Eng. Process.* **2018**, *132*, 105−113.
(11) Gašpariková, E.; Kapusta, Š.; Bodík, I.; Derco, J.; Kratochvíl, K.Evaluation of Anaerobic-Aerobic Wastewater Treatment Plant Operations. *Polish J. Environ. Stud.* **2005**, *14*, 12934
(12) Allabakshi, S. M.; Srikar, P. S. N. S. R.; Gangwar, R. K.; Maliyekkal, S. M. Feasibility of Surface Dielectric Barrier Discharge in Wastewater Treatment: Spectroscopic Modeling, Diagnostic, and Dye Mineralization. *Sep. Purif. Technol.* **2022**, *296* (March), No. 121344.
(13) Wang, Y.; Zhao, G.; Chai, S.; Zhao, H.; Wang, Y. Three-Dimensional Homogeneous Ferrite-Carbon Aerogel: One Pot Fabrication and Enhanced Electro-Fenton Reactivity. *ACS Appl. Mater. Interfaces* **2013**, *5* (3), 842−852.
(14) Lim, S.; Shi, J. L.; von Gunten, U.; McCurry, D. L. Ozonation of Organic Compounds in Water and Wastewater: A Critical Review. *Water Res.* **2022**, *213*, No. 118053.
(15) Shekhawat, S. S.; Gupta, A. B.; Kulshreshtha, N. M.; Prakash, R. UV Disinfection Studies on Chlorine Tolerant Bacteria Recovered from Treated Sewage. *J. Environ. Chem. Eng.* **2021**, *9* (3), No. 105253.
(16) Pignatello, J. J.; Oliveros, E.; MacKay, A. Advanced Oxidation Processes for Organic Contaminant Destruction Based on the Fenton Reaction and Related Chemistry. *Crit. Rev. Environ. Sci. Technol.* **2006**, *36* (1), 1−84.
(17) Glaze, W. H. Drinking-Water Treatment with Ozone. *Environ. Sci. Technol.* **1987**, *21* (3), 224−230.
(18) Rajeshwar, K. Solar Energy Conversion and Environmental Remediation Using. *J. Phys. Chem. Lett.* **2011**, *2*, 1301−1309.
(19) Pandis, P. K.; Kalogirou, C.; Kanellou, E.; Vaitsis, C.; Savvidou, M. G.; Sourkouni, G.; Zorpas, A. A.; Argirusis, C. Key Points of Advanced Oxidation Processes (AOPs) for Wastewater, Organic Pollutants and Pharmaceutical Waste Treatment: A Mini Review. *ChemEngineering* **2022**, *6* (1), 8.
(20) Ahlawat, K.; Jangra, R.; Ish, A.; Dixit, A.; Fulwani, D.; Jain, N.; Prakash, R. Analysis of a UV Photocatalytic Oxidation-Based Disinfection System for Hydroxyl Radicals, Negative Air Ions Generation and Their Impact on Inactivation of Pathogenic Micro-organisms. *Rev. Sci. Instrum.* **2023**, *94* (10), 104103.
(21) Tijani, J. O.; Fatoba, O. O.; Madzivire, G.; Petrik, L. F. A Review of Combined Advanced Oxidation Technologies for the Removal of Organic Pollutants from Water. *Water, Air, Soil Pollut.* **2014**, *225* (9), 1−30, DOI: 10.1007/s11270-014-2102-y.
(22) Rodríguez-Chueca, J.; Carbajo, J.; García-Muñoz, P. Intensification of Photo-Assisted Advanced Oxidation Processes for Water Treatment: A Critical Review. *Catalysts* **2023**, *13* (2), 1−36.
(23) Prevot, A. B.; Baiocchi, C.; Brussino, M. C.; Marc, G.; Palmisano, L. Photocatalytic Degradation of Acid Blue 80 in Aqueous Solutions Containing TiO2 Suspensions. *Environ. Sci. Technol.* **2001**, *35*, 971−976.
(24) Vinodgopal, K.; Wynkoop, D. E.; Kamat, P. V. Environmental Photochemistry on Semiconductor Surfaces: Photosensitized Degradation of a Textile Azo Dye, Acid Orange 7, on TiO2 Particles Using Visible Light. *Environ. Sci. Technol.* **1996**, *30* (5), 1660−1666.
(25) Borchers, H.; Fuller, A.; Malley, J. P. *Assessing the Risk of Mercury in Drinking Water after UV Lamp Breaks*; 2008.
(26) Amos, H. M.; Jacob, D. J.; Kocman, D.; Horowitz, H. M.; Zhang, Y.; Dutkiewicz, S.; Horvat, M.; Corbitt, E. S.; Krabbenhoft, D. P.; Sunderland, E. M. Global Biogeochemical Implications of Mercury Discharges from Rivers and Sediment Burial. *Environ. Sci. Technol.* **2014**, *48*, 9514 DOI: 10.1021/es502134t.
(27) Prakash, R.; Hossain, A. M.; Pal, U. N.; Kumar, N.; Khairnar, K.; Mohan, M. K. Dielectric Barrier Discharge Based Mercury-Free Plasma UV-Lamp for Efficient Water Disinfection. *Sci. Rep.* **2017**, *7* (1), 1−8.
(28) Joseph, A.; Vijayanandan, A. Review on Support Materials Used for Immobilization of Nano-Photocatalysts for Water Treatment Applications. *Inorg. Chim. Acta* **2023**, *545*, No. 121284.
(29) Teixeira, S.; Martins, P. M.; Lanceros-Méndez, S.; Kühn, K.; Cuniberti, G. Reusability of Photocatalytic TiO 2 and ZnO Nanoparticles Immobilized in Poly(Vinylidene Difluoride)-Co-Trifluoroethylene. *Appl. Surf. Sci.* **2016**, *384*, 497−504.
(30) Chang, C. Y.; Wu, N. L. Process Analysis on Photocatalyzed Dye Decomposition for Water Treatment with TiO2-Coated Rotating Disk Reactor. *Ind. Eng. Chem. Res.* **2010**, *49* (23), 12173−12179.
(31) Vaiano, V.; De Marco, I. Removal of Azo Dyes from Wastewater through Heterogeneous Photocatalysis and Supercritical Water Oxidation. *Separations* **2023**, *10* (4), 230.
(32) Vu, T. T.; del Río, L.; Valdés-Solís, T.; Marbán, G. Stainless Steel Wire Mesh-Supported ZnO for the Catalytic Photodegradation of Methylene Blue under Ultraviolet Irradiation. *J. Hazard. Mater.* **2013**, *246−247*, 126−134.
(33) Sun, L.; Bolton, J. R. Determination of the Quantum Yield for the Photochemical Generation of Hydroxyl Radicals in TiO2 Suspensions. *J. Phys. Chem.* **1996**, *100* (10), 4127−4134.
(34) Aristizábal, A.; Perilla, G.; Lara-Borrero, J. A.; Diez, R. KrCl and XeCl Excilamps and LP-Hg Lamp for UV and UV/H2O2 Decolourization of Dyes in Water. *Environ. Technol. (United Kingdom)* **2020**, *41* (2), 238−250.
(35) Liu, B.; Mullen, L.; Payne, E. M.; Linden, K. G. Accelerated Ultraviolet Treatment of Carbamazepine and NDMA in Water under 222 Nm Irradiation. *Environ. Sci. Technol.* **2023**, *47*, 18909.
(36) Murcia, M. D.; Gómez, M.; Gómez, E.; Gómez, J. L.; Christofi, N. Photodegradation of Congo Red Using XeBr, KrCl and Cl2 Barrier Discharge Excilamps: A Kinetics Study. *Desalination* **2011**, *281* (1), 364−371.
(37) Murcia, M. D.; Gómez, M.; Gómez, E.; Gomez, J. L.; Hidalgo, A. M.; Murcia, S.; Campos, D. Comparison of Two Excilamps and Two Reactor Configurations in the UV-H2O2 Removal Process of Amaranth. *J. Water Process Eng.* **2020**, *33*, No. 101051.
(38) Allabakshi, S. M.; Srikar, P. S. N. S. R.; Gangwar, R. K.; Maliyekkal, S. M. Feasibility of Surface Dielectric Barrier Discharge in Wastewater Treatment: Spectroscopic Modeling, Diagnostic, and Dye Mineralization. *Sep. Purif. Technol.* **2022**, *296* (March), No. 121344.
(39) Ahlawat, K.; Jangra, R.; Ish, A.; Jain, N.; Prakash, R. A Dielectric Barrier Discharge Based Low Pressure Narrow Band Far UV-C 222 Nm Excimer Lamp and Its Efficiency Analysis. *Phys. Scr.* **2024**, *99* (2), No. 025018.
(40) Wang, X.; Sø, L.; Su, R.; Wendt, S.; Hald, P.; Mamakhel, A.; Yang, C.; Huang, Y.; Iversen, B. B.; Besenbacher, F. The Influence of Crystallite Size and Crystallinity of Anatase Nanoparticles on the Photo-Degradation of Phenol. *J. Catal.* **2014**, *310*, 100−108.

https://doi.org/10.1021/acsomega.4c00516
ACS Omega 2024, 9, 15615−15632

(41) Chen, H.; Nanayakkara, C. E.; Grassian, V. H. Titanium Dioxide Photocatalysis in Atmospheric Chemistry. *Chem. Rev.* **2012**, *112* (11), 5919−5948.
(42) Ahlawat, K.; Jangra, R.; Chaturvedi, S.; Prakash, C.; Dixit, A.; Fulwani, D.; Gupta, A.; Jain, N.; Tak, V.; Prakash, R. Photocatalytic Oxidation Conveyor " PCOC " System for Large Scale Surface Disinfection. *Rev. Sci. Instrum.* **2022**, *93*, No. 074101, DOI: 10.1063/5.0082222.
(43) Jangra, R.; Ahlawat, K.; Prakash, R. An SDBD Plasma-Based Source for Efficient Degradation of VOCs in an Enclosed Environment. *Phys. Lett. A* **2023**, *490*, No. 129184.
(44) Makuła, P.; Pacia, M.; Macyk, W. How To Correctly Determine the Band Gap Energy of Modified Semiconductor Photocatalysts Based on UV-Vis Spectra. *J. Phys. Chem. Lett.* **2018**, *9* (23), 6814−6817.
(45) Allabakshi, S. M.; Srikar, P. S. N. S. R.; Gangwar, R. K.; Maliyekkal, S. M. Treatment of Azo, Direct, and Reactive Dyes in Surface Dielectric Barrier Discharge: Valorization of Effluent, the Influence of Wastewater Characteristics, and Plasma Modeling by Stark Broadening Technique. *J. Water Process Eng.* **2023**, *56* (June), No. 104503.
(46) Asgari, G.; Salari, M.; Molla Mahmoudi, M.; Jamshidi, R.; Dehdar, A.; Faraji, H.; Zabihollahi, S.; Alizadeh, S. Kinetic Studies of Dexamethasone Degradation in Aqueous Solution via a Photocatalytic UV/H2O2/MgO Process. *Sci. Rep.* **2022**, *12* (1), 1−11.
(47) Reza, K. M.; Kurny, A.; Gulshan, F. Parameters Affecting the Photocatalytic Degradation of Dyes Using TiO2: A Review. *Appl. Water Sci.* **2017**, *7*, 1569−1578, DOI: 10.1007/s13201-015-0367-y.
(48) Jangra, R.; Ahlawat, K.; Dixit, A.; Prakash, R. Efficient Deactivation of Aerosolized Pathogens Using a Dielectric Barrier Discharge Based Cold - Plasma Detergent in Environment Device for Good Indoor Air Quality. *Sci. Rep.* **2023**, *13*, 1−14.
(49) Chatterley, C.; Linden, K. Demonstration and Evaluation of Germicidal UV-LEDs for Point-of-Use Water Disinfection. *J. Water Health* **2010**, *8* (3), 479−486.
(50) Khan, I.; Saeed, K.; Khan, I. Nanoparticles: Properties, Applications and Toxicities. *Arab. J. Chem.* **2019**, *12* (7), 908−931.
(51) Reddy, K. M.; Manorama, S. V.; Reddy, A. R. Bandgap Studies on Anatase Titanium Dioxide Nanoparticles. *Mater. Chem. Phys.* **2003**, *78* (1), 239−245.
(52) Pawar, M.; Sendoğdular, S. T.; Gouma, P. A Brief Overview of TiO2 Photocatalyst for Organic Dye Remediation: Case Study of Reaction Mechanisms Involved in Ce-TiO2 Photocatalysts System. *J. Nanomater.* **2018**, *2018*, 5953609 DOI: 10.1155/2018/5953609.
(53) Bharti, B.; Kumar, S.; Lee, H. N.; Kumar, R. Formation of Oxygen Vacancies and Ti3+ State in TiO2 Thin Film and Enhanced Optical Properties by Air Plasma Treatment. *Sci. Rep.* **2016**, *6* (May), 1−12.
(54) Cottre, T.; Fingerle, M.; Kranz, M.; Mayer, T.; Kaiser, B.; Jaegermann, W. Interaction of Water with Atomic Layer Deposited Titanium Dioxide on P-Si Photocathode: Modeling of Photoelectrochemical Interfaces in Ultrahigh Vacuum with Cryo-Photoelectron Spectroscopy. *Adv. Mater. Interfaces* **2021**, *8* (11), 2002257 DOI: 10.1002/admi.202002257.
(55) Kritikos, D. E.; Xekoukoulotakis, N. P.; Psillakis, E.; Mantzavinos, D. Photocatalytic Degradation of Reactive Black 5 in Aqueous Solutions: Effect of Operating Conditions and Coupling with Ultrasound Irradiation. *Water Res.* **2007**, *41* (10), 2236−2246.
(56) Toor, A. T.; Verma, A.; Jotshi, C. K.; Bajpai, P. K.; Singh, V. Photocatalytic Degradation of Direct Yellow 12 Dye Using UV/TiO2 in a Shallow Pond Slurry Reactor. *Dye. Pigment.* **2006**, *68* (1), 53−60.
(57) Liu, C. C.; Hsieh, Y. H.; Lai, P. F.; Li, C. H.; Kao, C. L. Photodegradation Treatment of Azo Dye Wastewater by UV/TiO2 Process. *Dye. Pigment.* **2006**, *68* (2−3), 191−195.
(58) Tang, C.; Chen, V. The Photocatalytic Degradation of Reactive Black 5 Using TiO2/UV in an Annular Photoreactor. *Water Res.* **2004**, *38* (11), 2775−2781.
(59) Sohrabi, M. R.; Ghavami, M. Photocatalytic Degradation of Direct Red 23 Dye Using UV/TiO2: Effect of Operational Parameters. *J. Hazard. Mater.* **2008**, *153* (3), 1235−1239.
(60) Azizian, S. Kinetic Models of Sorption: A Theoretical Analysis. *J. Colloid Interface Sci.* **2004**, *276* (1), 47−52.
(61) Muruganandham, M.; Sobana, N.; Swaminathan, M. Solar Assisted Photocatalytic and Photochemical Degradation of Reactive Black 5. *J. Hazard. Mater.* **2006**, *137* (3), 1371−1376.
(62) Rai, P. K.; Kant, V.; Sharma, R. K.; Gupta, A. Process Optimization for Textile Industry-Based Wastewater Treatment via Ultrasonic-Assisted Electrochemical Processing. *Eng. Appl. Artif. Intell.* **2023**, *122*, No. 106162.
(63) Abdellah, M. H.; Nosier, S. A.; El-Shazly, A. H.; Mubarak, A. A. Photocatalytic Decolorization of Methylene Blue Using TiO2/UV System Enhanced by Air Sparging. *Alexandria Eng. J.* **2018**, *57* (4), 3727−3735.
(64) Luo, M.; Xu, W.; Jeong, T. Development and Numerical Modelling of a Novel UV/H2O2rotating Flow Reactor for Water Treatment. *Water Sci. Technol.* **2021**, *83* (5), 1217−1229.
(65) Bilal, M.; Rasheed, T.; Iqbal, H. M. N.; Hu, H.; Wang, W.; Zhang, X. Toxicological Assessment and UV/TiO2-Based Induced Degradation Profile of Reactive Black 5 Dye. *Environ. Manage.* **2018**, *61* (1), 171−180.
(66) Sannino, D.; Morante, N.; Sacco, O.; Mancuso, A.; De Guglielmo, L.; Di Capua, G.; Femia, N.; Vaiano, V. Visible Light-Driven Degradation of Acid Orange 7 by Light Modulation Techniques. *Photochem. Photobiol. Sci.* **2023**, *22* (1), 185−193.
(67) Butman, M. F.; Gushchin, A. A.; Ovchinnikov, N. L.; Gusev, G. I.; Zinenko, N. V.; Karamysheva, S. P.; Krämer, K. W. Synergistic Effect of Dielectric Barrier Discharge Plasma and TiO2-Pillared Montmorillonite on the Degradation of Rhodamine B in an Aqueous Solution. *Catalysts* **2020**, *10* (4), 359.
(68) Zhang, X.; Shi, P.; Zhao, W.; Lu, W.; Li, F.; Min, Y.; Xu, Q. Research on Methylene Blue Degradation Based on Multineedle-to-Plane Liquid Dielectric Barrier Discharge Mode. *Sep. Purif. Technol.* **2022**, *286*, No. 120476, DOI: 10.1016/j.seppur.2022.120476.
(69) Jiang, S. Y.; Ma, A.; Ramachandran, S. Negative Air Ions and Their Effects on Human Health and Air Quality Improvement. *Int. J. Mol. Sci.* **2018**, *19* (10), 2966.
(70) Luts, A.; Salm, J. Chemical Composition of Small Atmospheric Ions near the Ground. *J. Geophys. Res.: Atmos.* **1994**, *99*, 781−785.
(71) Verlackt, C. C. W.; Van Boxem, W.; Bogaerts, A. Transport and Accumulation of Plasma Generated Species in Aqueous Solution. *Phys. Chem. Chem. Phys.* **2018**, *20* (10), 6845−6859.
(72) Lu, X.; Naidis, G. V.; Laroussi, M.; Reuter, S.; Graves, D. B.; Ostrikov, K. Reactive Species in Non-Equilibrium Atmospheric-Pressure Plasmas: Generation, Transport, and Biological Effects. *Phys. Rep.* **2016**, *630* (April), 1−84.
(73) Wang, Y.; Song, H.; Chen, J.; Chai, S.; Shi, L.; Chen, C.; Wang, Y.; He, C. A Novel Solar Photo-Fenton System with Self-Synthesizing H2O2: Enhanced Photo-Induced Catalytic Performances and Mechanism Insights. *Appl. Surf. Sci.* **2020**, *512*, No. 145650.
(74) Deng, Y.; Zhao, R. Advanced Oxidation Processes (AOPs) in Wastewater Treatment. *Curr. Pollut. Reports* **2015**, *1* (3), 167−176.
(75) Plum, A.; Braun, G.; Rehorek, A. Process Monitoring of Anaerobic Azo Dye Degradation by High-Performance Liquid Chromatography-Diode Array Detection Continuously Coupled to Membrane Filtration Sampling Modules. *J. Chromatogr. A* **2003**, *987* (1−2), 395−402.
(76) El Bouraie, M.; El Din, S. W. Biodegradation of Reactive Black 5 by Aeromonas Hydrophila Strain Isolated from Dye-Contaminated Textile Wastewater. *Sustain. Environ. Res.* **2016**, *26*, 209.
(77) Sun, D.; Zhang, X.; Du, H.; Fang, L.; Jiang, P. Application of Liquid Organic Salt to Cotton Dyeing Process with Reactive Dyes. *Fibers Polym.* **2017**, *18* (10), 1969−1974.
(78) Zhao, L.; Sun, Y.; Qiu, R.; Sun, H.; Feng, J. Application of Liquid Film Dielectric Barrier Discharge Plasma Reactor in the Degradation of Rhodamine B: Performance Optimization, Mechanism and Pathways. *J. Water Process Eng.* **2022**, *50*, No. 103231.
(79) Nurnaeimah, N.; Mat, N.; Mohd, K. S.; Badaluddin, N. A.; Yusoff, N.; Sajili, M. H.; Mahmud, K.; Adnan, A. F. M.; Khandaker, M. M. The Effects of Hydrogen Peroxide on Plant Growth, Mineral

https://doi.org/10.1021/acsomega.4c00516
ACS Omega 2024, 9, 15615−15632

Accumulation, as Well as Biological and Chemical Properties of Ficus Deltoidea. *Agronomy* **2020**, *10* (4), 599.
(80) Jafariyan, T.; Zarea, M. J. Hydrogen Peroxide Affects Plant Growth Promoting Effects of Azospirillum. *J. Crop Sci. Biotechnol.* **2016**, *19* (2), 167−175.
(81) Sivachandiran, L.; Khacef, A. Enhanced Seed Germination and Plant Growth by Atmospheric Pressure Cold Air Plasma: Combined Effect of Seed and Water Treatment. *RSC Adv.* **2017**, *7* (4), 1822−1832.
(82) Cuerda-Correa, E. M.; Alexandre-Franco, M. F.; Fernández-González, C. Advanced Oxidation Processes for the Removal of Antibiotics from Water. An Overview. *Water* **2020**, *12* (1), 102.

https://doi.org/10.1021/acsomega.4c00516
ACS Omega 2024, 9, 15615−15632